J. Fluid Mech. (1981), *vol.* 107, *pp.* 1–35
Printed in Great Britain

Oscillating flow over steep sand ripples

By MICHAEL S. LONGUET-HIGGINS

Department of Applied Mathematics and Theoretical Physics, Silver Street, Cambridge, *and* Institute of Oceanographic Sciences, Wormley, Surrey

(Received 4 July 1980)

Although the form and dimensions of steep vortex ripples are well studied in relation to the oscillating flow which generates them, nevertheless the accompanying fluid motion is not yet understood quantitatively. In this paper we present a method of calculation based on the assumption that the sand–water interface is fixed and that the effect of sand in suspension is, to a first approximation, negligible.

The method employs a simple conformal transformation of the fluid flow onto the exterior of a polygon, and thence onto the interior of a unit circle. The initial, irrotational flow is represented by a logarithmic vortex at the centre of the circle. Other vortices within the fluid are each represented by a symmetric system of P vortices and their images in the unit circle, P being the number of sides of the original polygon. Typically P is equal to 5. However, P is not limited to integer values but may be any rational number greater than 2 (see § 15).

To proceed with the calculation it is assumed that separation of the boundary layer takes place at the sharp crests of the ripples, and that the shed vorticity can be represented by discrete vortices, with strengths given by Prandtl's rule. (For a typical time sequence see figures 7 and 8.) After a complete cycle, a *vortex pair* is formed, which can escape upwards from the neighbourhood of the boundary.

The total momentum per ripple wavelength and the horizontal force on the bottom are expressible very simply in terms of the shed vortices at any instant. The force consists of two parts: an added-mass term which dissipates no energy, and a 'vortex drag', which extracts energy from the oscillating flow.

The calculation is at first carried out with point vortices, in a virtually inviscid theory. However, it is found appropriate to assume that each vortex has a solid core whose radius *expands with time* like $[\epsilon(t-t_n)]^{\frac{1}{2}}$, where t_n denotes the time of birth, and ϵ is a small parameter analogous to a viscosity. The expansion of the vortex tends to reduce the total energy (which otherwise would increase without limit) at a rate independent of ϵ. If the cores of two neighbouring vortices overlap they are assumed to merge, by certain simple rules.

Calculation of the effective vortex drag in an oscillating flow yields drag coefficients $\bar{C}_D$ of the order of 10^{-1}, in good agreement with the measurements of Bagnold (1946) and of Carstens, Nielson & Altinbilek (1969). The tendency for the highest drag coefficients to occur when the ratio $2a/L$ of the total horizontal excursion of the particles to the ripple length is about 1·5 is confirmed. When $2a/L = 4$, the drag falls to about half its value at 'resonance'.

1. Introduction

Regularly spaced ripples are a common feature of sandy sea beds along many coasts. Usually they are found just seawards of the swash zone, and their intimate connexion with wave action and with the mechanisms of sediment suspension and transport by waves and nearshore currents has long been suspected.

The spacing and the form of sand ripples in relation to wave action have been the subject of many thorough investigations, for example by Bagnold (1946), Inman (1957), Carstens *et al.* (1969), Mogridge & Kamphuis (1972) and Lofquist (1978). A recent summary and discussion of the literature has been given by Nielson (1979). Some striking relationships appear. For example

(1) the ripple length (the spacing between adjacent crests) is generally about two-thirds of the horizontal excursion of the water particles, independently of the frequency of oscillation and hence of the Reynolds number;

(2) the ripple length is almost independent of the sand-grain density;

(3) the mean drag coefficients are remarkably high, being of order 10^{-1}, nearly two orders of magnitude greater than for steady flows over a rough bottom.

On the other hand, it seems that a quantitative understanding of the conditions under which steep ripples are formed and maintained by oscillatory waves is still lacking, due chiefly to difficulties in calculating the time-dependent motion of the fluid.

In a general way, it was recognized as early as Ayrton (1910) that the formation of steep sand ripples is connected with the existence of a system of vortices thrown off at the crests of the ripples, in alternate directions. During the forward 'stroke' of the fluid motion, a vortex is formed in the lee of each ripple crest, which picks up sand from the trough and from the lee slope of the ripples, subsequently depositing it on the ripple crests. Thus the ripples and vortices cooperate; at each stroke the vortices act to repair the previous erosion of the ripple crests, and a remarkably stable situation persists. The process has been well described by Bagnold (1946, §4).

In the course of this phenomenon, a considerable amount of the sediment may be taken into suspension (particularly with small grain-sizes). This material can then be transported in either direction according to the characteristics of the waves or mean current that is present (see Bijker, van Hijum & Vellinga 1976).

Attempts to calculate the fluid flow were made by Kalkanis (1964) and by Kajiura (1968), but these authors assumed an essentially flat solid boundary between sand and water. More recently Sleath (1975) has carried out numerical calculations of the flow over an undulating bed, assuming laminar flow conditions, appropriate to low Reynolds numbers. While achieving some successes, this method is clearly not applicable to conditions at high Reynolds numbers where the boundary layers are not well resolved by the numerical technique. In Sleath (1975) the crests of the ripples are assumed to be more rounded than the troughs. Though it is possible to reverse this assumption, and make the model crests sharper, nevertheless they still cannot be made as sharp as those of ripples under formative wave action. In such circumstances we expect separation of the boundary layer at a well-defined point, namely the sharp crest itself.

The present paper attacks the problem of the flow over ripples by a different method. There are two new aspects to our technique. First, we make a simple transformation of

a typical sequence of a ripple-forms into the sides of a regular polygon, as described in §2 below. From there it is comparatively simple to map the domain of the flow (which corresponds to the *exterior* of the polygon) onto the interior of the unit circle (see §3). The transformation is altogether similar to that used by the present author (1973) to approximate the flow beneath a progressive gravity wave in deep water, except that here it is not the interior of the polygon but the exterior which is mapped onto the unit circle.

If the flow were irrotational, this mapping would immediately give the velocity field over the ripple (see §4). The second main feature of our method is that we assume the actual flow field, in which the boundary layer separates at the ripple crests, to be represented by a distribution of point vortices, with circulation given by Prandtl's rule, as in §6. Each vortex is then represented in the transformed plane by a simple circular vortex together with its image in the unit circle (see figure 5). The motion of the vortices and of the corresponding velocity field may then be calculated by straightforward time-stepping.

Such a method of computation by 'surface vorticity' has been used recently by Clements (1973), Stansby (1977), Graham (1980) and others, to calculate the shedding of vortices from circular or sharp-edged cylinders in steady and oscillating flow. A historical review is given by Clements & Maull (1975); see also Saffman & Baker (1979). The method is practical so long as the requisite number of vortex elements is not too great. In the present application the number of vortices is brought within practical bounds by some amalgamation into single vortices or, more interestingly, into *vortex pairs* which can escape from the neighbourhood of the boundary.

One advantage of the present method is the very simple expression for the total horizontal momentum, derived in §7 below, and for the resulting stress on the ripple surface, derived in §8. These enable our computations to be readily compared with laboratory observations by Bagnold (1946), Carstens *et al.* (1969) and Lofquist (1980), with excellent agreement.

2. The polygon transformation

Consider a sequence of ripples, each of length L, as in figure 1 (a), and let

$$z = x + iy, \tag{2.1}$$

where x and y are rectangular co-ordinates, the origin is at a crest A, the x axis is horizontal and the y axis vertically upwards.

Suppose first that the interior angle at the crest of each ripple is $(\pi - 2\pi/P)$, where P is an integer. To fix the ideas we may take $P = 5$, so that the crest angle is 108°. Then by the simple transformation

$$\zeta = e^{-ikz}, \quad kPL = 2\pi, \tag{2.2}$$

any P consecutive vertices of the ripple are transformed into the vertices of a regular P-gon (polygon with P sides) as shown in figure 1 (b). The vertex $z = 0$ goes to the point $\zeta = 1$, and points at infinite depth ($y = -\infty$) go to the origin $\zeta = 0$ in figure 1 (b).

The transformation (2.2) being conformal, angles are preserved locally, so that the transformed boundary in figure 1 (b) also has an interior angle $(\pi - 2\pi/P)$ at each corner. This being the interior angle of a regular P-gon it follows that the trans-

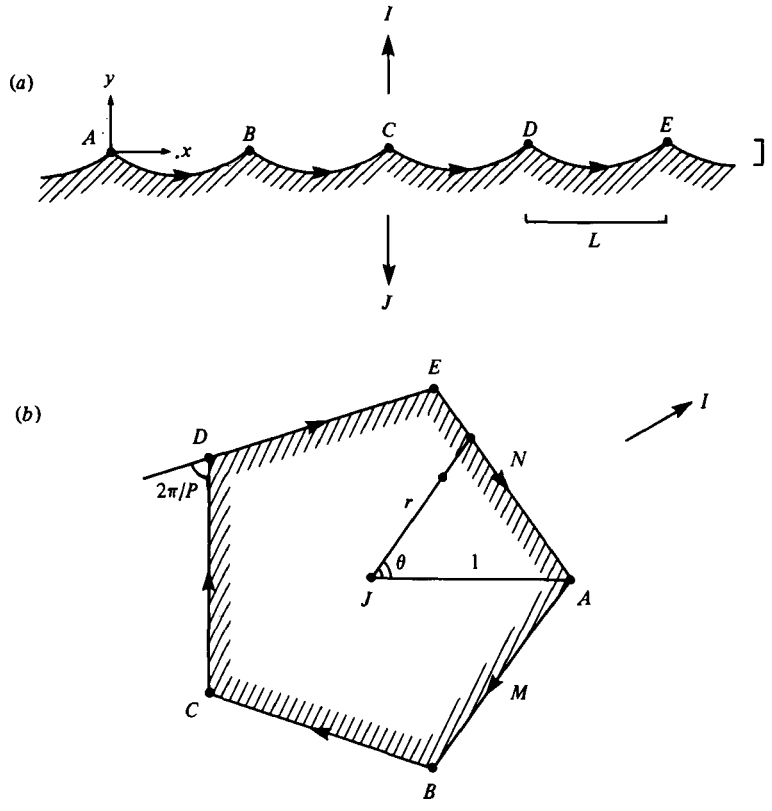

FIGURE 1. A sequence of ripple profiles (*a*) in the z plane and (*b*) transformed into a polygon in the ζ plane.

formed boundary touches the sides of the P-gon at each vertex. Accordingly we approximate the transformed boundary by the sides of the P-gon itself. The sand and the water are then represented by the interior and the exterior of the P-gon respectively.

The equation of the boundary, in the ζ plane, is given by

$$r\cos(\theta-\theta_j) = \cos(\pi/P), \tag{2.3}$$

where r and θ are polar co-ordinates (see figure 2) and θ_j is one of the P angles

$$2\pi(j-\tfrac{1}{2})/P, \quad j = 1, 2, \ldots P.$$

On transforming back into the physical plane by

$$kz = i\ln\zeta = i\ln r - \theta, \tag{2.4}$$

we find for the equation of the ripple surface in the z plane

$$k(y-y_0) = \ln\sec k(x-x_0), \tag{2.5}$$

where x_0 and y_0 are constants, and $|k(x-x_0)| \leqslant \pi/P$. The ripple steepness, that is the ratio of its crest-to-trough height h to the ripple length L, is given by

$$\frac{h}{L} = \frac{\ln\sec(\pi/P)}{2\pi/P}. \tag{2.6}$$

Values of this expression for some low values of P are shown in table 1. For typical profiles see figure 2.

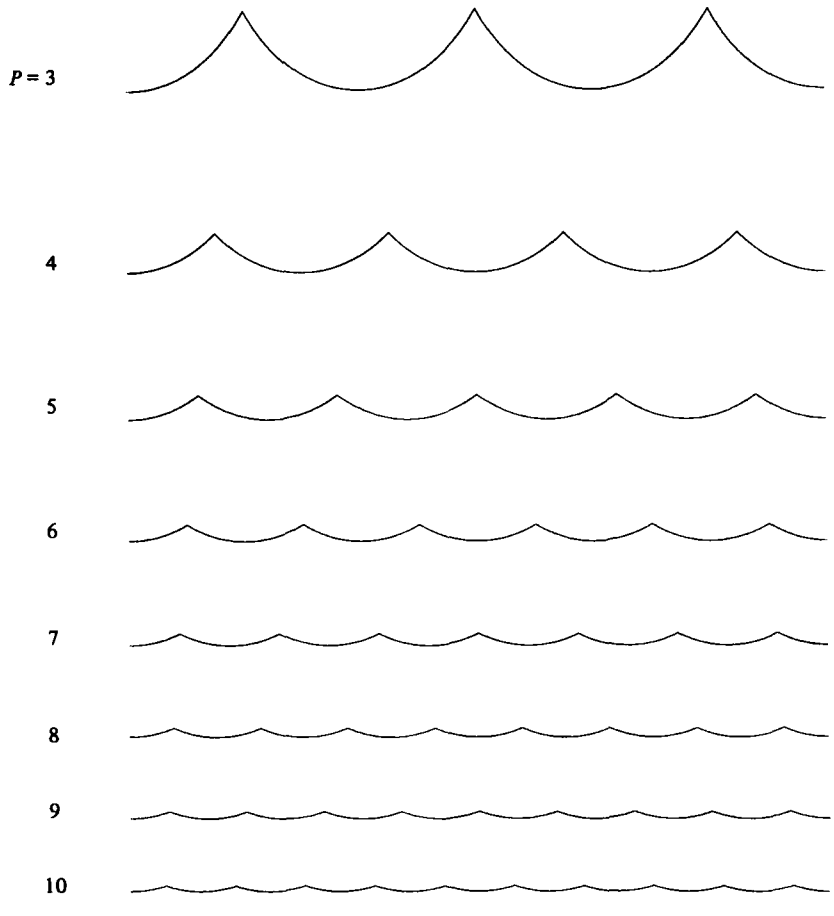

FIGURE 2. Typical sequences of profiles given by equation (2.5).

P	π/P	h/L	K	m	μ
2	90°	∞	·500000	∞	∞
5/2	72°	·4673	·639696	·848757	·727596
3	60°	·3310	·730499	·484595	·379120
7/2	$51\frac{3}{7}°$	·2632	·791737	·325257	·238897
4	45°	·2206	·834627	·236547	·165803
5	36°	·1687	·888855	·143323	·094115
6	30°	·1374	·920371	·096825	·060863
7	$25\frac{5}{7}°$	·1162	·940223	·070010	·042646
8	$22\frac{1}{2}°$	·1008	·953506	·053063	·031564
10	18°	·0799	·969597	·033567	·019307
12	15°	·0662	·978591	·023166	·013026

TABLE 1. Parameters of the polygon transformation.

Actual ripple steepnesses usually lie between about 0·09 and 0·21 (see Nielsen 1979), the most common values being $0{\cdot}18 \pm 0{\cdot}02$. This suggests that a value $P = 5$ is not unrealistic. In fact the profile (2.5) is then extremely close to the 'normal' form† of the ripple as indicated by Lofquist (1978, figure 26). We shall therefore adopt this value of P for most of the subsequent numerical work. However, we emphasize that the analysis is by no means confined to this value of P, or even to P integral (see §11).

The 'normal' shape of ripple is related to the 'angle of repose' of the sand grains. This commonly is close to the maximum surface slope of the ripple. The angle of repose is in turn related to the shape of the sand grains, which again is correlated with their mean size (the smaller grains being on the whole more rounded). This has led Nielsen (1979) to suggest a correlation between ripple steepness and grain size.

Nielsen (1979) also suggested approximating the profile of each ripple by a parabola. The corresponding velocity field would be quite difficult to analyse. However, by using the alternative form (2.5) we shall obtain a comparatively simple expression for the flow over the ripple.

3. Mapping onto a circle

It is straightforward to map the exterior of the polygon in figure 1(*b*) onto the *interior* of the unit circle in figure 3 by writing

$$\zeta = \zeta_0 - K\int_{W_0}^{W} \frac{(1-W^P)^{2/P}}{W^2}\,dW, \tag{3.1}$$

where ζ_0, W_0 and K are constants, to be determined. Equation (3.1) is the form to which the Schwartz–Christoffel transformation (Nehari 1952) reduces when the vertices of the original P-gon are transformed into the points

$$W = e^{2ij\pi/P}, \quad j = 1, 2, \ldots, P \tag{3.2}$$

on the unit circle. The lower limit of integration W_0 in (3.1) may be chosen arbitrarily in or on the unit circle (excepting at the origin). The constant K defines the scale of the transformation.

To determine K, we may take $W_0 = 1$ and $W = e^{2i\pi/P}$ in figure 3. The corresponding points A, B in figure 1*b* are $\zeta_0 = 1$ and $\zeta = e^{-2i\pi/P}$. So from (3.1) we have

$$K = (1-e^{-2i\pi/P}) \div \int_1^{e^{2i\pi/P}} \frac{(1-W^P)^{2/P}}{W^2}\,dW. \tag{3.3}$$

Evaluation of the definite integral in (3.3) yields

$$K = \frac{\sin(\pi/P)}{2^{2/P}} \frac{\Gamma(1/P)}{\Gamma(\frac{1}{2})\Gamma(\frac{1}{2}+1/P)} = \frac{(1/P)!}{(2/P)!\,(-1/P)!}. \tag{3.4}$$

Some values of K are given in the fourth column of table 1.

† 'Normal' in the sense of not 'compressed' or 'extended'.

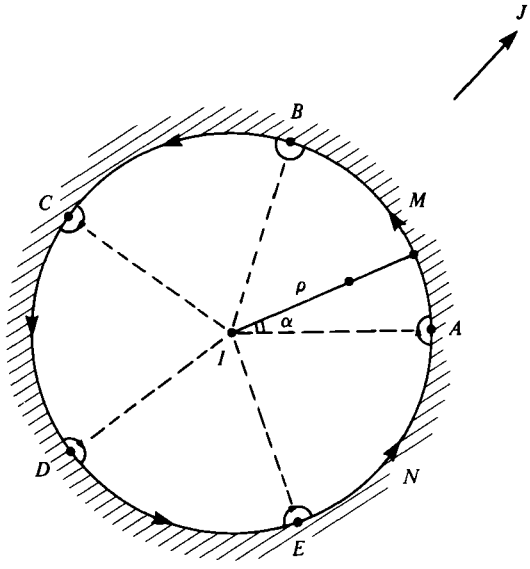

FIGURE 3. Transformation of the domain of flow in figure 1 onto the interior of the unit circle in the W plane.

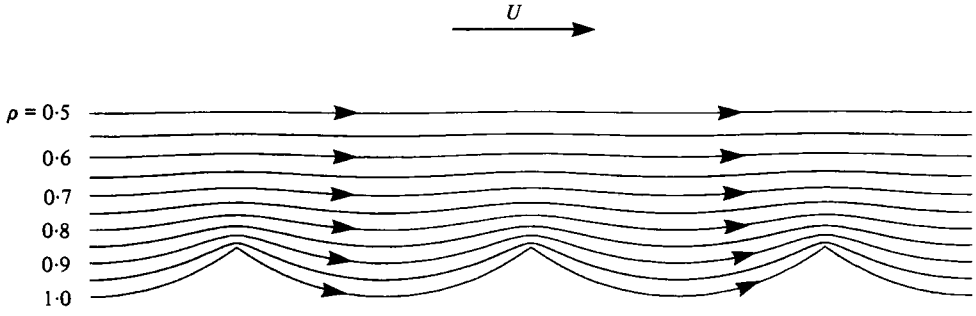

FIGURE 4. Streamlines in the z plane corresponding to the initial irrotational flow.

To clarify the transformation further, we set

$$W = \rho e^{i\alpha}, \tag{3.5}$$

so that $\rho = 1$ corresponds to the unit circle. As a point in the z plane follows the profile of a ripple from A to B in the positive sense (x increasing) the corresponding point ζ in figure 1(*b*) traverses one side AB of the polygon in the clockwise (i.e. negative) sense, and the corresponding point W in figure 3 describes an arc AB of the unit circle in the anticlockwise (i.e. positive) sense. In each case the sand is on the right and the fluid on the left.

For numerical computation it is convenient to take $W_0 = e^{-i\pi/P}$ to avoid the singularity at $W = 1$. Figure 4 shows some curves $\rho =$ constant calculated in this way. These correspond to concentric circles in the W plane.

4. The initial flow

Suppose the fluid above the ripple is started from rest impulsively, in such a way that far above the surface the flow is a uniform horizontal stream of strength U. Initially the flow will be irrotational and so is described by a velocity potential $\chi = \phi + i\psi$ such that as $y \to \infty$ so

$$\chi \sim Uz. \tag{4.1}$$

Then from (4.1) and (2.2)

$$\chi \sim (iU/k)\ln\zeta. \tag{4.2}$$

But from (3.1) we have when W is small

$$\zeta \sim K/W. \tag{4.3}$$

Hence (4.2) becomes, as $W \to 0$,

$$\chi \sim (U/ik)\ln W. \tag{4.4}$$

Now the potential

$$\chi = (U/ik)\ln W, \tag{4.5}$$

represents a circular vortex in the W plane having zero flow across the boundary $\rho = 1$. It is regular everywhere except at $W = 0$, where it has the required asymptotic behaviour, by (4.4). Therefore (4.5) represents the required initial flow.

The streamlines correspondong to (4.5) are given by

$$\psi = -(U/k)\ln\rho, \tag{4.6}$$

and so are represented by the curves $\rho =$ constant in figure 4.

5. The flow due to a vortex

Consider next the flow due to a vortex of strength Γ imbedded in the fluid at the point $z = z_n$, say. Because of periodicity in the x direction, we assume there are similar vortices at the points $z = z_n \pm jL$, $j = 1, 2, \ldots$.

The situation in the W plane is shown in figure 5. If W_n is the point corresponding to z_n, there will be a vortex of strength Γ at each of the points

$$W = W_n e^{2\pi j i\alpha/P}, \quad j = 1, \ldots, P. \tag{5.1}$$

Now the velocity potential associated with a single vortex at W_n is

$$\frac{\Gamma}{2\pi i}\ln(W - W_n). \tag{5.2}$$

The potential associated with all P vortices in the interior is accordingly

$$\sum_{j=1}^{P}\frac{\Gamma}{2\pi i}\ln(W - W_n e^{2\pi j i/P}) = \frac{\Gamma}{2\pi i}\ln(W^P - W_n^P). \tag{5.3}$$

In order to satisfy the condition of zero flow across the unit circle we simply add P vortices of equal but opposite strength $-\Gamma$ at the image points

$$\overline{W}_n = 1/W_n^* \tag{5.4}$$

etc. where a star denotes the complex conjugate. Thus altogether we have

$$\chi = \frac{\Gamma}{2\pi i}\ln\frac{W^P - W_n^P}{W^P - \overline{W}_n^P}. \tag{5.5}$$

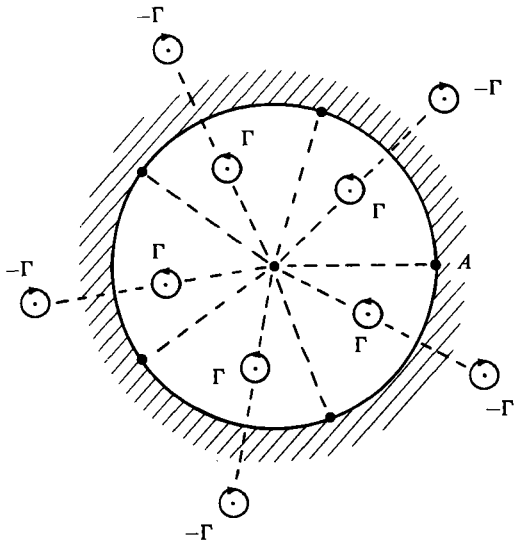

FIGURE 5. A system of vortices and their images in the unit circle $|W| = 1$.

Consider now the motion of each vortex. For a free vortex we have, in the z plane,

$$\frac{dz_n^*}{dt} = \frac{d}{dz}\left[\chi - \frac{\Gamma}{2\pi i}\ln(z-z_n)\right]_{z\to z_n}. \tag{5.6}$$

For the corresponding motion in the W plane we have

$$\frac{dW_n^*}{dt} = W_n'^* \frac{dz_n^*}{dt}, \tag{5.7}$$

where W' denotes dW/dz. From (5.6) and (5.7) we have

$$\begin{aligned}\frac{dW_n^*}{dt} &= W_n' W_n'^* \frac{d}{dW}\left[\chi - \frac{\Gamma}{2\pi i}\ln(z-z_n)\right] \\ &= |W_n'|^2\left[\frac{d\chi}{dW} - \frac{\Gamma}{2\pi i}\frac{1}{W'(z-z_n)}\right].\end{aligned} \tag{5.8}$$

It is convenient to introduce the modified potential

$$\chi^{(n)} = \chi - \frac{\Gamma}{2\pi i}\ln(W-W_n). \tag{5.9}$$

Near $z = z_n$, an expansion in Taylor series gives

$$(W-W_n) = W'(z-z_n)\left[1+\frac{1}{2}\frac{W''}{W'}(z-z_n)\right] \tag{5.10}$$

and so

$$\frac{1}{W'(z-z_n)} = \frac{1}{W-W_n} + \frac{W''}{2W'^2}. \tag{5.11}$$

From (5.8) and (5.9) we have therefore

$$\frac{dW_n^*}{dt} = |W_n'|^2\left[\frac{d\chi^{(n)}}{dW} - \frac{\Gamma}{2\pi i}\frac{W''}{2W'^2}\right]. \tag{5.12}$$

In (5.12) the last term depends essentially on the *curvature* of the mapping function $W(z)$.

In (5.12) it is easy now to calculate the value of $d\chi^{(n)}/dW$ at $W = W_n$. If χ is given by (5.5) we find

$$\frac{d\chi^{(n)}}{dW} = \frac{\Gamma}{2\pi i}\left[\frac{P-1}{2W_n} - \frac{PW_n^{P-1}}{W_n^P - \overline{W}_n^P}\right] = \frac{\Gamma}{2\pi i}\frac{(P-1)+(P+1)\rho_n^{2P}}{2W_n(1-\rho_n^{2P})}, \tag{5.13}$$

where $\rho_n = |W_n|$. From (2.2) and (3.1) we have also

$$W' = \frac{d\zeta}{dz}\frac{dW}{d\zeta} = \frac{ik\zeta W^2}{K(1-W^P)^{2/P}}, \tag{5.14}$$

and hence

$$\frac{W''}{2W'^2} = \frac{1}{2W'}\frac{dW'}{dW} = \frac{k}{2iW'} + \frac{1}{W(1-W^P)}. \tag{5.15}$$

6. Vortex shedding

After the initial motion, boundary layers will form at the surface of the ripple. If q denotes the tangential velocity within the boundary layer, and η is a co-ordinate normal to the boundary, the flux of vorticity within the layer is $q\,\partial q/\partial\eta$. Assuming q to vanish on the boundary itself, the total vorticity flux across the layer is then

$$\int q(\partial q/\partial\eta)\,d\eta = \tfrac{1}{2}Q^2, \tag{6.1}$$

where Q is the velocity just outside the boundary layer (see Prandtl & Tietjens 1934). Thus at the point of separation, vorticity will be shed from the boundary layer at a rate $\frac{1}{2}Q^2$.

Following Clements (1973) and others, we shall agree to represent the resulting motion by a succession of vortices imbedded in the irrotational flow, each vortex being of strength

$$\Gamma_n = \int \tfrac{1}{2}Q^2\,dt, \tag{6.2}$$

where the integral is taken over the time since shedding of the previous vortex.

The initial position of each vortex is assumed to be given by

$$z_n = z_0 + \int u\,dt, \tag{6.3}$$

where z_0 is at or near the point of separation and u is the corresponding vector velocity, so $Q = |u|$.

At any given time, therefore, the flow will be represented by a potential of the form

$$\chi = (U/ik)\ln W + \sum_n \frac{\Gamma_n}{2\pi i}\ln\frac{W^P - W_n^P}{W^P - \overline{W}_n^P}. \tag{6.4}$$

At points other than the vortices themselves the velocity will be given by

$$u^* = \frac{d\chi}{dz} = W'\frac{d\chi}{dW}, \tag{6.5}$$

that is

$$u^* = \frac{W'}{W}\left[\frac{U}{ik} + \sum_n \frac{\Gamma_n}{2\pi i}\left(\frac{PW^P}{W^P - W_n^P} - \frac{PW^P}{W^P - \overline{W}_n^P}\right)\right]. \tag{6.6}$$

The motion of the vortices themselves is found from §5:

$$\frac{dW_n^*}{dt} = \frac{|W_n'|^2}{W_n}\left[\frac{U}{ik} + \frac{\Gamma_n}{2\pi i}\left\{\frac{(P-1)+(P+1)\rho_N^{2P}}{2(1-\rho_n^{2P})} - \frac{W_n W_n''}{2W_n'^2}\right\} + \sum_{m\neq n}\frac{\Gamma_m}{2\pi i}\left\{\frac{PW_n^P}{W_n^P - W_m^P} - \frac{PW_n^P}{W_n^P - \overline{W}_m^P}\right\}\right]. \tag{6.7}$$

7. The total momentum

Expressions for the total momentum and for the net force exerted on the boundary turn out to be remarkably simple.

The total linear momentum, or impulse I, of a body of fluid contained within a contour C is given in general (see Ramsey 1942) by

$$I = -\int_C \psi\, dz, \tag{7.1}$$

where ψ is the stream function, and we have taken the fluid density to be unity. ψ is assumed single-valued and non-singular within C. Any singularities at z_n, say, must be enclosed by contours B_n surrounding z_n and joined to C, if ψ is not single-valued. In the case of the potential (6.4) ψ is in fact single-valued everywhere but at the points z_n, and the contributions to I from the small contours surrounding these singularities are vanishingly small.

Consider then the momentum contained in the contour C as defined by figure 6. The contour consists of part of the ripple surface C_1, two vertical lines C_2 and C_4 at $x = \pm\frac{1}{2}L$, and a remote horizontal line C_3 on which $y = y_\infty$ and $\psi \sim \psi_\infty$, say.

Take first the contribution I_U from the term in χ proportional to U. For this we have

$$\psi = -(U/k)\ln\rho. \tag{7.2}$$

On C_1 we have $\rho = 1$ so ψ vanishes. From C_2 and C_4 together there is no net contribution, by the periodicity of ρ as a function of x. Therefore altogether

$$I_U = -\int_{C_3}\psi\, dz = \int_{-\frac{1}{2}L}^{\frac{1}{2}L}\psi_\infty dx = -(UL/k)\ln\rho_\infty. \tag{7.3}$$

Now from (2.2) and (4.4) we have

$$ky_\infty = \mathrm{Re}\,(\ln\zeta) = \ln(K/\rho_\infty) \tag{7.4}$$

and so

$$\ln\rho_\infty = \ln K - ky_\infty. \tag{7.5}$$

Therefore altogether we have as the contribution to I from the current at infinity

$$I_U = UL(y_\infty - k^{-1}\ln K). \tag{7.6}$$

This expression is of course real, the vertical component of the momentum being zero.

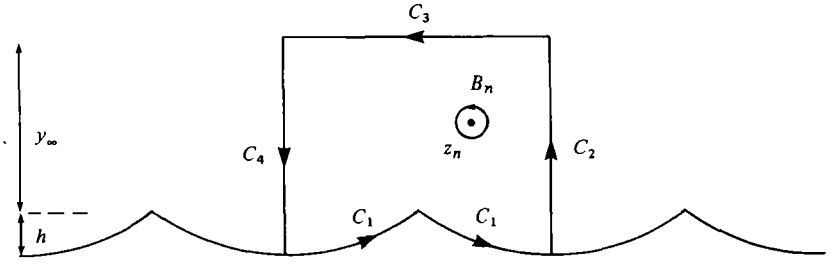

FIGURE 6. The contour C of integration in the z plane.

We note that the total mass M of water contained below the level $y = y_\infty$ is given by

$$M = L(y_\infty + k^{-1}m), \tag{7.7}$$

where

$$m = \frac{1}{L}\int_{x=-\frac{1}{2}L}^{\frac{1}{2}L} x\,d(\ln\sec kx)$$
$$= \frac{P}{2\pi}\int_{-\pi/P}^{\pi/P} \xi\tan\xi\,d\xi. \tag{7.8}$$

Values of m are given in table 1. m/k represents the mean thickness of the water contained below the level of the ripple crests.

Consider now the contribution to I from each vortex. From (6.4)

$$\psi = -\frac{\Gamma_n}{2\pi}\ln\left|\frac{W^P - W_n^P}{\overline{W}^P - \overline{W}_n^P}\right|. \tag{7.9}$$

On C_1, ψ is constant and equal to

$$-\frac{\Gamma_n}{2\pi}\ln\left|\frac{1-\rho_n^P}{1-\rho_n^{-P}}\right| = -\frac{\Gamma_n}{2\pi}\ln\rho_n^P. \tag{7.10}$$

The contribution to I is therefore

$$-\int_{C_1}\psi\,dz = \frac{LP}{2\pi}\Gamma_n\ln\rho_n. \tag{7.11}$$

The contributions from C_2 and C_4 cancel by periodicity, while on C_3, where W is small, we have

$$\psi = -\frac{\Gamma_n}{2\pi}\ln(W_n/\overline{W}_n)^P = -\frac{\Gamma_n}{2\pi}\ln\rho_n^{2P}. \tag{7.12}$$

The contribution from C_3 is thus minus twice the contribution from C_1. Noting that

$$\frac{LP}{2\pi} = \frac{1}{k}, \tag{7.13}$$

we have altogether

$$I_V = -k^{-1}\sum_n \Gamma_n\ln\rho_n. \tag{7.14}$$

For vortices shed by a positive current, the circulation Γ_n is generally clockwise, or negative. Since $\rho_n \leqslant 1$, this means that I_V will be negative in general, i.e. each vortex produces a *momentum defect* proportional to its strength Γ_n. It is useful to consider each vortex together with its image; really it is the image which induces the negative momentum.

Altogether, from (7.6) and (7.14) we have

$$I = UL(y_\infty - k^{-1}\ln K) - k^{-1}\sum_n \Gamma_n \ln \rho_n. \tag{7.15}$$

8. The force on the boundary

From the above expressions we can immediately calculate the net force F exerted on the ripple surface, either in steady or time-dependent flow. For, suppose the fluid is accelerated by a mean horizontal pressure-gradient $\varpi = (\partial p/\partial x)_{y=\infty}$. From the motion at infinity we have

$$\varpi = -\frac{dU}{dt}. \tag{8.1}$$

Now, considering the balance of horizontal momentum contained within the contour C of figure 6, we note that the convection of momentum across both C_1 and C_3 vanishes, while the convection across C_2 just cancels that across C_4, by the x periodicity. The rate of change of the momentum within C is therefore due solely to the pressure applied at the boundaries. Now the net force on the water across C_1 equals $-F$. At z on C_2 the pressure p exceeds the pressure at the corresponding point $(z-L)$ on C_4 by an amount $L\varpi$ precisely, so the net force across these two boundaries is

$$-L\varpi(h+y_\infty), \tag{8.2}$$

where h is the height of the ripple. Lastly the contribution from the horizontal contour C_3 vanishes. The momentum balance therefore gives

$$\frac{dI}{dt} = -F - L\varpi(h+y_\infty), \tag{8.3}$$

or by (8.1)

$$F = -\frac{dI}{dt} + L\frac{dU}{dt}(h+y_\infty). \tag{8.4}$$

On substituting for I from (7.15) we obtain finally

$$kF = L\frac{dU}{dt}(kh + \ln K) + \frac{d}{dt}\sum_n \Gamma_n \ln \rho_n. \tag{8.5}$$

The first term in equation (8.5), namely

$$kF_U = L\frac{dU}{dt}(kh + \ln K) \tag{8.6}$$

can be considered as resulting from an added mass μ/k per unit horizontal distance, where

$$\mu = kh + \ln K = \ln(K\sec \pi/P). \tag{8.7}$$

This quantity is given in table 1. Clearly the force F_U is proportional to dU/dt. In an oscillating flow it does, on the whole, no work.

The second term in (8.5), namely

$$kF_V = \frac{d}{dt}\sum_n \Gamma_n \ln \rho_n, \tag{8.8}$$

represents a mean stress

$$\tau_V = F_V/L = \frac{P}{2\pi}\frac{d}{dt}\sum_n \Gamma_n \ln \rho_n, \tag{8.9}$$

due to the generation and propagation of the vortices. In those time intervals when no new vortices are being generated, both the Γ_n and the number of terms under the summation remain constant and (8.8) reduces to

$$kF_V = \sum_n \Gamma_n \dot{\rho}_n / \rho_n, \tag{8.10}$$

a formula that can be verified by Blasius' theorem (see appendix A). Generally, however, allowance must be made in F_V for the generation of new vortices at the point of separation.

Consider now the rate of working D by the external pressure gradient, per unit horizontal distance. This is

$$D = -\int_{-h}^{y_\infty} w \frac{\partial \psi}{\partial y}\, dy = w(\psi_s - \psi_\infty), \tag{8.11}$$

where ψ_s denotes the value of ψ on the surface of the ripple. The part of ψ involving U makes no net contribution, as we have seen. We therefore have left the vortex contribution alone. From (8.11), (7.11) and (7.13),

$$D = -\frac{dU}{dt} \sum_n \frac{P\Gamma_n}{2\pi} \ln \rho_n. \tag{8.12}$$

In time-periodic motion, the right-hand side of (8.12) may be replaced, on average, by

$$D = U \frac{d}{dt} \sum_n \frac{P\Gamma_n}{2\pi} \ln \rho_n, \tag{8.13}$$

that is to say

$$D = U\tau_V, \tag{8.14}$$

where τ_V is given by equation (8.9). In other words, the mean rate of working by the external pressure gradient is just that required to overcome the vortex-induced stress on the bottom. Thus we have an energy balance, despite the fact that the self-energy of the vortices is infinite.

9. Numerical computations

The method outlined above is well suited to numerical computation in FORTRAN with complex arithmetic.

As first step, a subroutine was constructed yielding z as a function of W using equations (2.4) and (3.1). The values of K in table 1, which were first derived from (3.4) using tabulated values of the gamma function (Abramowitz & Stegun 1965) were then checked by means of the formula

$$K = i \sin(2\pi/P) \div \int_{\exp(-i\pi/P)}^{\exp(i\pi/P)} \frac{(1 - W^P)^{2/P}}{W^2}\, dW, \tag{9.1}$$

in which the lower limit W_0 is taken as $e^{-i\pi/P}$, in order to avoid the singularity at $W = 1$. The values of K in table 1 were verified in this way to six significant figures.

To carry out the method of § 6 a basic time-step Δt was chosen, of order 0·05 or less, the velocity at infinity being given by

$$U = \begin{cases} 0, & t \leqslant 0, \\ U_0 \sin \sigma t, & t \geqslant 0. \end{cases} \tag{9.2}$$

In most computations σ was chosen as unity (the results for inviscid fluid being independent of the time scale) and further

$$U_0 = 0{\cdot}75L\omega, \tag{9.3}$$

where L is the ripple length. Again, units of length were chosen so that

$$k = 1, \quad L = 2\pi/P \tag{9.4}$$

and in most of the computations P was taken to equal 5 (see § 2).

At the jth time-step t_j it was supposed that the position W_n of the nth vortex in the W plane was advanced by an amount

$$\Delta W_n = \begin{cases} \dot{W}_n(t_j)\,\Delta t, & j = 1, \\ [\frac{3}{2}\dot{W}_n(t_j) - \frac{1}{2}\dot{W}_n(t_{j-1})]\,\Delta t, & j = 2, 3, \ldots, \end{cases} \tag{9.5}$$

the latter formula being accurate to $O(\Delta t)^3$, not $(\Delta t)^2$. The values of $\dot{W}_n = dW_n/dt$ were calculated from equation (6.7).

After every three time-steps a new vortex was generated at the point

$$W_N = W_0 + \sum_j W_0' u_j^* \,\Delta t, \tag{9.6}$$

where W_0 is the point $(1-\delta)$ close to the ripple crest $W = 1$, and u_j denotes the velocity at W_0 (found from equation (6.6)) at the three preceding instants t_j where $j = (3N-2)$, $(3N-1)$, $3N$. The strength of the vortex was taken as

$$\Gamma_N = \tfrac{1}{2}\sum_j u_j u_j^* \,\Delta t, \tag{9.7}$$

corresponding to equation (6.2). The value of δ was taken as 0·1.

When programmed in FORTRAN on the IBM 370–95 at Cambridge University, the above computation took about 3 min for 250 time-steps (up to $N = 83$). Thereafter each time-step took a time proportional nearly to the square of the number of vortices: N^2.

As was found by Clements (1973) and also by Kiya & Arie (1977), the results were fairly insensitive to the particular value of δ (representing boundary-layer thickness) and of the time-step Δt, except that if Δt were too large some vortices were lost by crossing the ripple boundary $\rho = 1$. To avoid this it was found necessary to keep Δt not greater than 0·025.

10. Initial results

Figure 7 shows successive stages of the computation for the sinusoidal oscillation given by equations (9.2) and (9.3), with $\delta = 0{\cdot}1$ and $\Delta t = 0{\cdot}025$. Each small semicircle represents a vortex, the radius R_n being proportional to the square root of the corresponding circulation, in fact

$$R_n = (0{\cdot}1\Gamma_n)^{\frac{1}{2}}. \tag{10.1}$$

The strength of each vortex is thus proportional to the *area* of the corresponding small circle. Negative and positive vorticity is represented by semicircles) and (, having gaps on their left and right sides, respectively.

In figure 7 (*c*) when $t = 0{\cdot}9$, the initial shear layer, represented by the 12 discrete

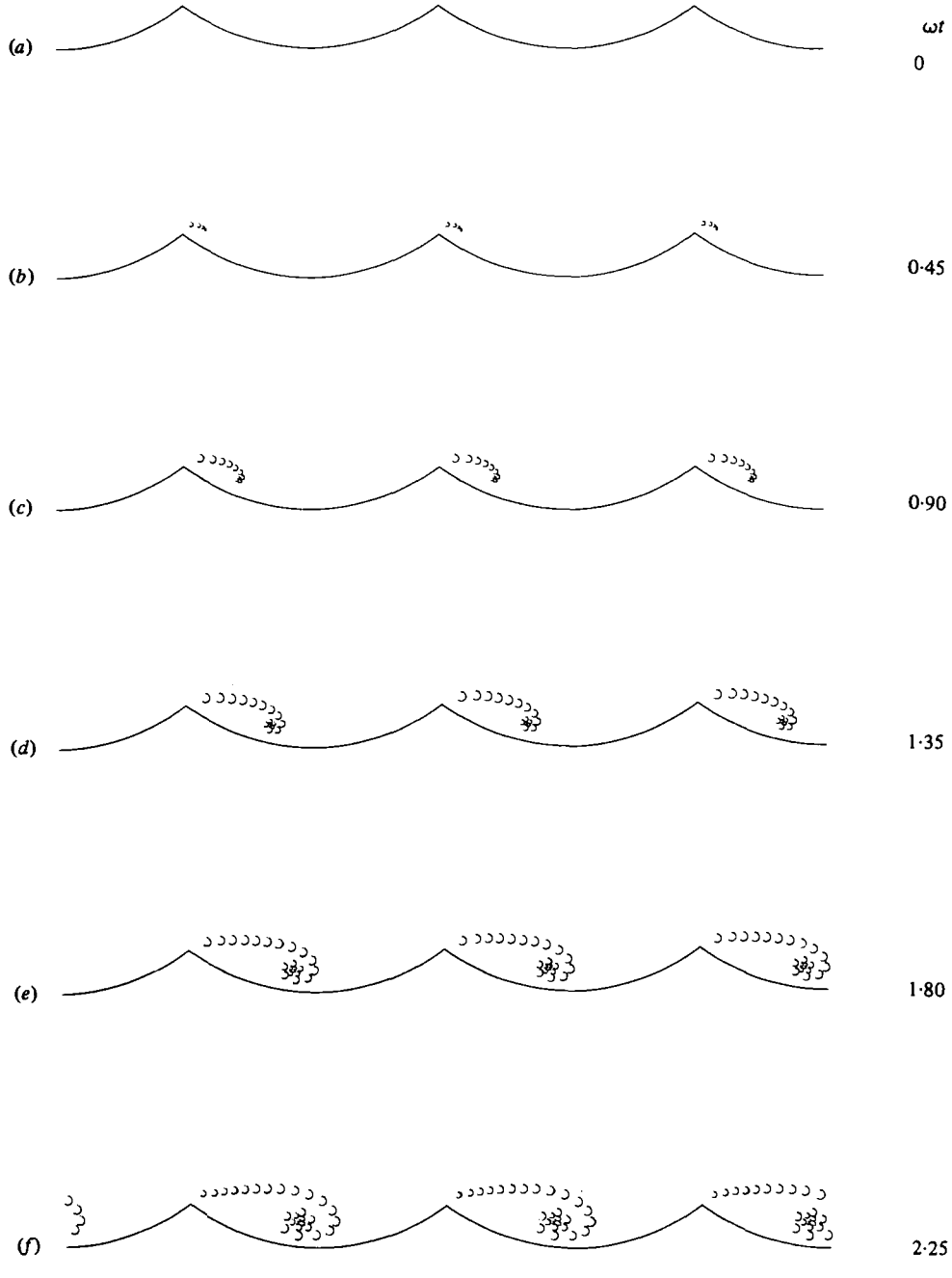

FIGURE 7. Successive positions of point vortices, in the sinusoidal flow $U = 0{\cdot}75 \sin \omega t$ starting from rest at time $t = 0$. The case $P = 5$, $\omega = 1$, $k = 1$, $\epsilon = 0$.

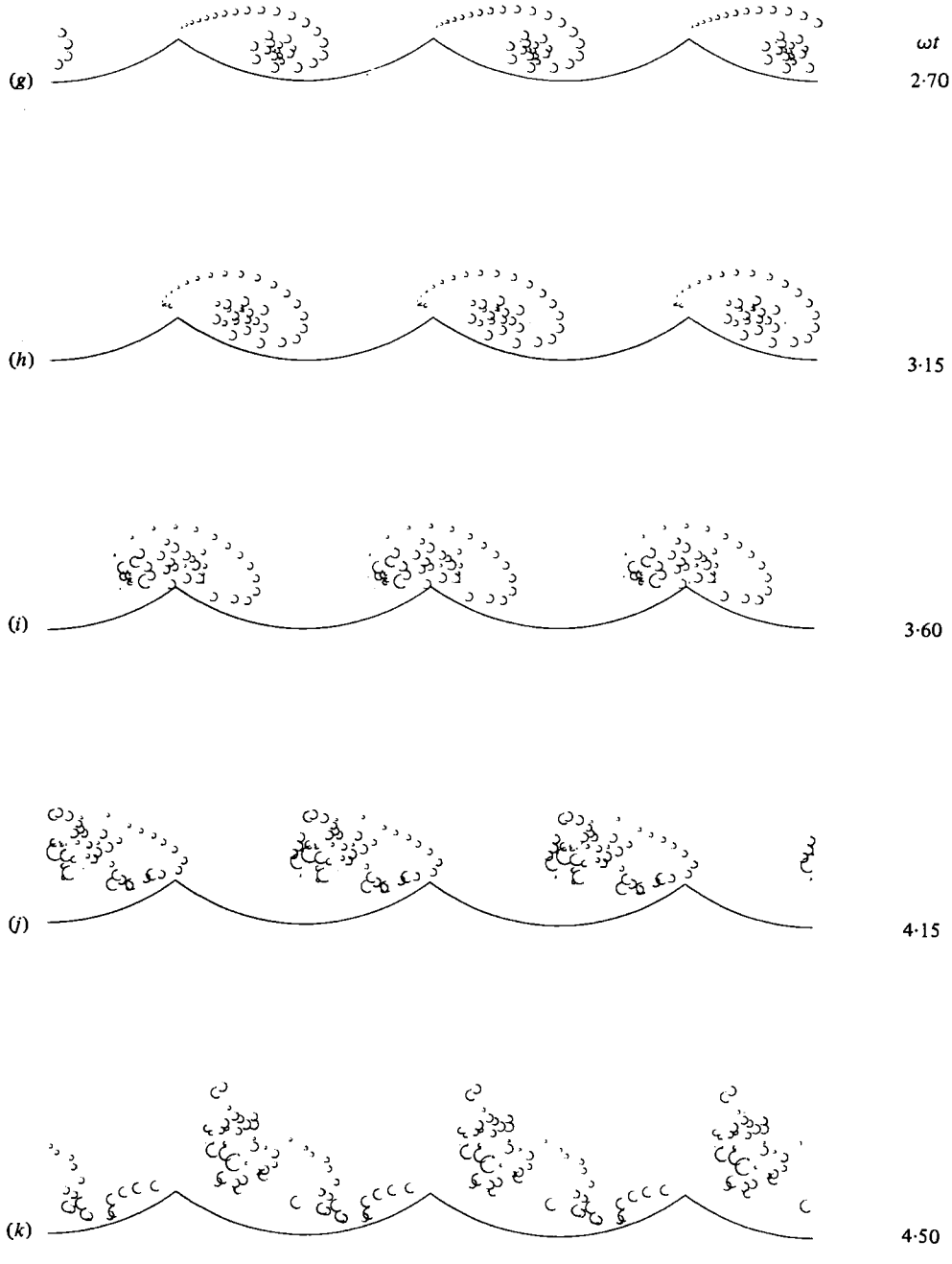

FIGURE 7 (*g–k*). For legend see p. 16.

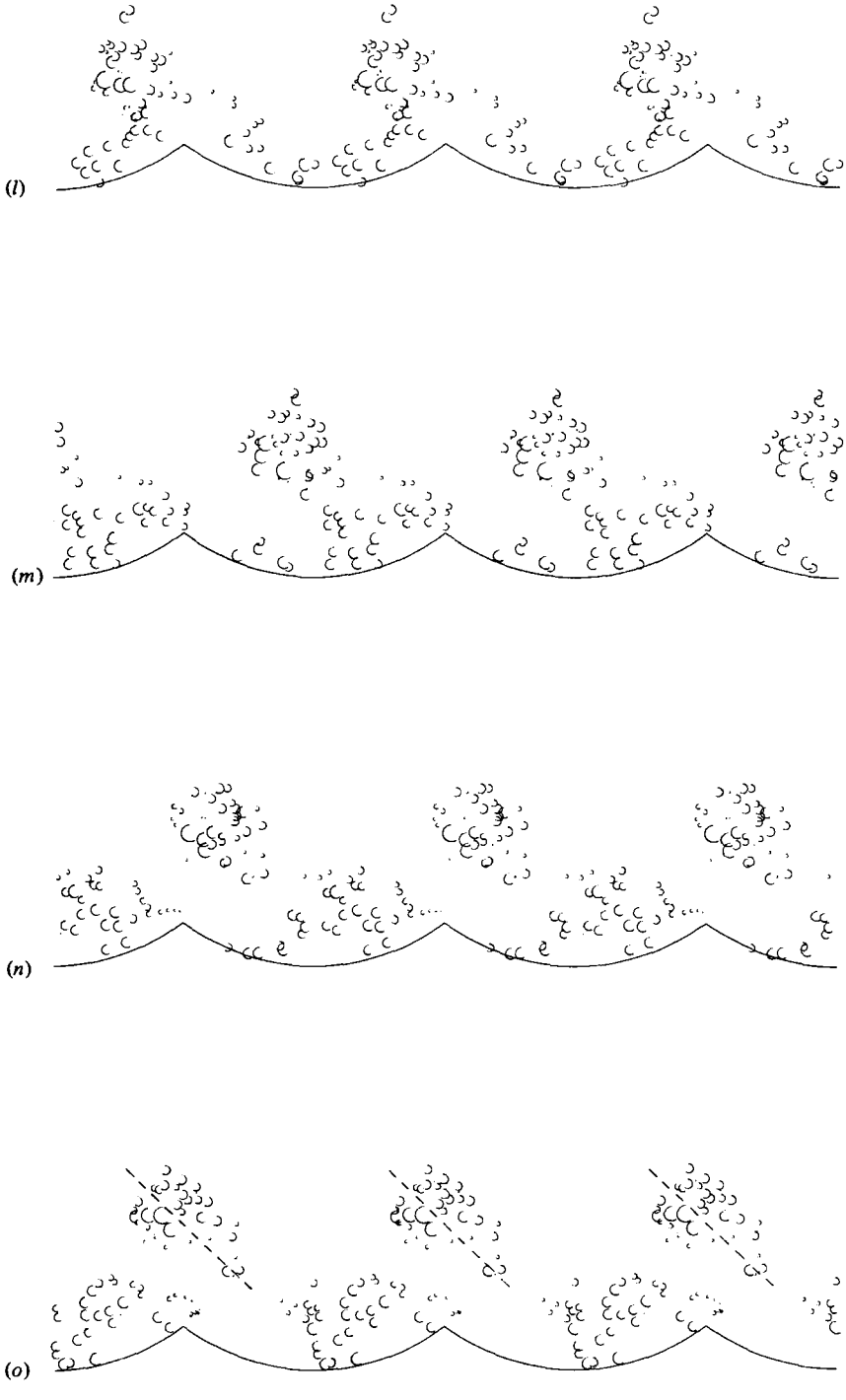

FIGURE 7 (*l–o*). For legend see p. 16.

vortices shed by this time, is beginning to curl over, under the influence of its own vorticity. When $t = 1{\cdot}80$ the process is further continued, the first 15 point vortices becoming concentrated into a rather tight spiral in the lee trough of the wave.

The greatest excursion of the vortices to the right occurs when $t \doteqdot 2{\cdot}7$. By this time the velocity U is slowing down, and the strength of the vortices shed at the crest is quite small. At $t = 3{\cdot}15 \doteqdot \pi$ the flow at the crest is already reversed and some vortices of the opposite sign are being shed. When $t = 3{\cdot}6$ the vortex is being swept back over the crest, dragging with it some vorticity of the opposite sign. Between $t = 3{\cdot}15$ and $t = 6{\cdot}30$ the initial vortex is carried back through a distance of $2\frac{1}{2}$ ripple lengths (though the total stroke $2a$ is only $1{\cdot}5L$) and comes almost to rest above the crest two ripple lengths to the left of its starting-point, having risen to a height of about $\frac{1}{2}L$.

When $t = 6{\cdot}3$, the clouds of vorticity above the crests have become detached from the fluid below, and it is possible to draw a line at about $y = 0{\cdot}25$ (the wavelength L being $2\pi/5$) separating these clouds from the vorticity remaining near the surface. On examining the 'clouds' more closely it can be seen that each of them is divided roughly into two halves, by an axis at 45° to the horizontal. Above the axis the vorticity has mainly the same sign as the original vortex, i.e. it is negative. Below the axis the vorticity is mainly positive. If now we sum the total positive circulation $\sum_{\Gamma>0} \Gamma_n$ within the cloud it is found to be 0·710, compared with the total negative vorticity, which is $-0{\cdot}712$. The total circulation in the cloud is therefore almost exactly zero, showing that the cloud is, in effect, a vortex pair. It is this property that has enabled the cloud to rise to its actual height and escape from the neighbourhood of the boundary.

(It will be recalled that an isolated irrotational vortex has infinite energy, not only on account of the motion near its centre, which can easily be replaced by a viscous core, but more significantly from the velocity field at infinity, which is proportional to $|z-z_n|^{-1}$. Thus in an infinite fluid to establish a single vortex would require infinite energy. But, in the presence of a plane boundary, an irrotational vortex, together with its image, has only finite energy, the cores being disregarded. A vortex and its image can therefore be more easily generated. At the same time such a vortex pair is trapped by the boundary; it cannot get away by itself without an infinite supply of energy. Suppose, however, that it meets another vortex pair, or system of vortices, such that the circulation of the total system on one side of the boundary is zero, then this system, or any part of it having zero combined circulation, may indeed escape.)

11. Vortex pairing

To proceed further it seems permissible, at this stage, to simplify the computation by replacing the upper clouds of vorticity in figure 7(*o*) by equivalent vortex pairs. Thus we wish to define two vortices Γ_+, Γ_-, say, situated at points W_+ and W_- in the W plane, with at least the following properties:

$$\Gamma_+ + \Gamma_- = \sum_n \Gamma_n \tag{11.1}$$

and

$$\Gamma_+ \ln W_+ + \Gamma_- \ln W_- = \sum_n \Gamma_n \ln W_n. \tag{11.2}$$

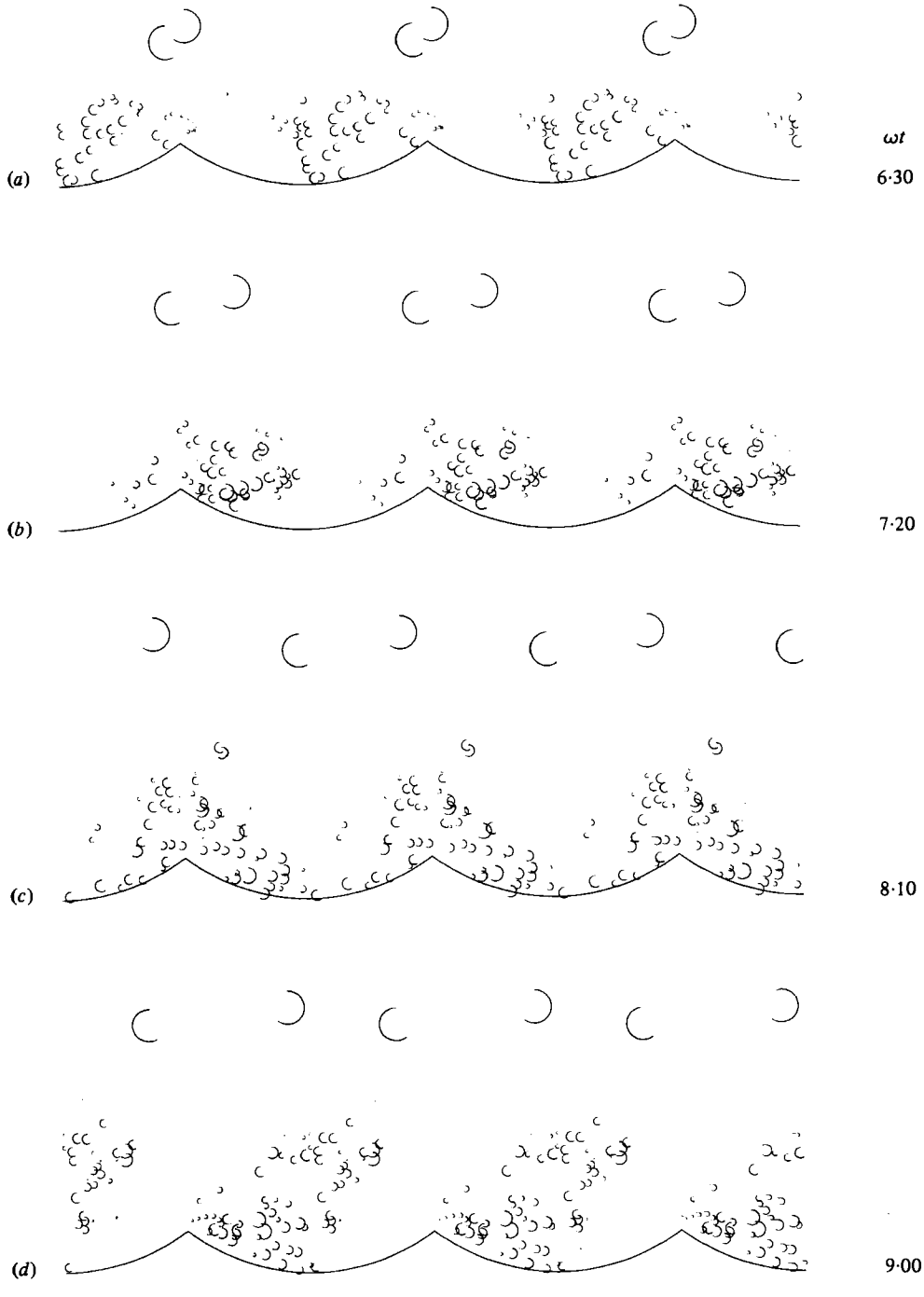

Figure 8. Positions of point vortices after consolidation of 'clouds' in figure 6 (*o*) into a vortex pair.

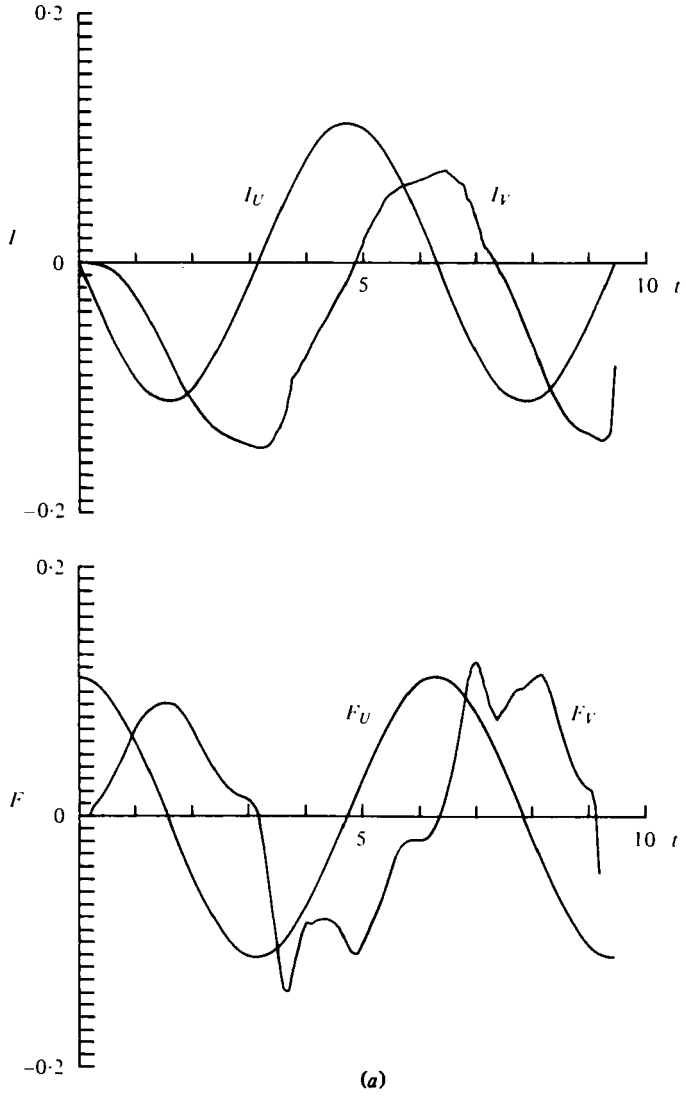

FIGURE 9. Comparison of the momentum I and vortex force F (*a*) without and (*b*) with consolidation of the vortex pair at time $t = 6{\cdot}30$. The case $P = 5$, $\omega = 1$, $k = 1$, $\epsilon = 0$.

The first property ensures that the total circulation of the system remains unaltered, and the second that the total momentum also is unchanged (see § 6), at least momentarily. To these conditions we may add the following:

$$|\Gamma_+| + |\Gamma_-| = \sum_n |\Gamma_n| \tag{11.3}$$

and

$$|\Gamma_+| \ln W_+ + |\Gamma_-| \ln W_- = \sum_n |\Gamma_n| \ln W_n \tag{11.4}$$

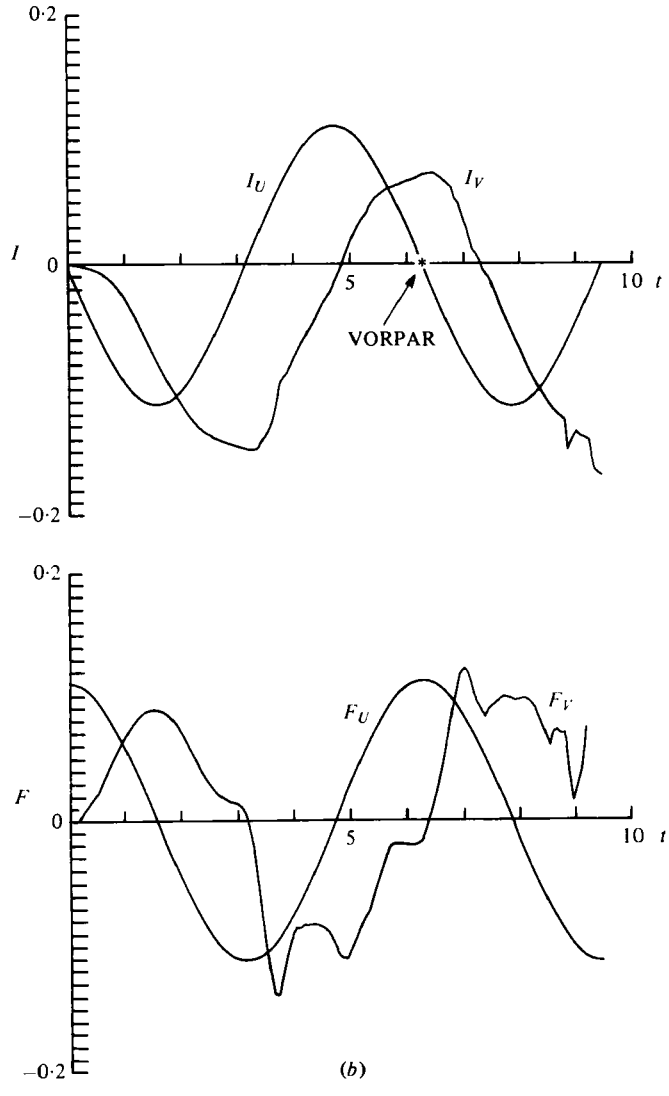

FIGURE 9(*b*). For legend see p. 21.

which, assuming Γ_+ and Γ_- are of opposite sign, serve with the two previous equations to define the vortices uniquely. In fact if the four sums in (11.1) to (11.4) are denoted by S_1, S_2, S_3 and S_4 respectively, and if $\Gamma_+ > 0$, we have

$$\left.\begin{aligned}\Gamma_+ &= \tfrac{1}{2}(S_1+S_3),\\ \Gamma_- &= \tfrac{1}{2}(S_1-S_3)\end{aligned}\right\} \tag{11.5}$$

and

$$\left.\begin{aligned}\ln W_+ &= (S_2+S_4)/(S_1+S_3),\\ \ln W_- &= (S_2-S_4)/(S_1-S_3).\end{aligned}\right\} \tag{11.6}$$

It is understood that the summations S_i are taken over the vortices of the cloud only.

When this is done, figure 7(*o*) is replaced by the corresponding figure 8(*a*). On

proceeding further (figures 8*b–d*) it is found that the new vortex pair rises to a height $y = 0{\cdot}8L$, well above the boundary. At the same time, interestingly, the original vortex pairs become separated, probably under the influence of the remaining vorticity below (compare Aref 1979) and each vortex forms a new pair with its neighbour on the other side.

Meanwhile each cloud of vorticity situated in the ripple troughs to the left of a crest in figure 8(*a*) moves to the right through a distance of nearly two wavelengths and rises to a height of about $0{\cdot}3\,L$, having picked up some opposite vorticity on the way.

If the total vorticity in the cloud above $y = 0{\cdot}25$ is summed it is again found to be roughly in balance with the total negative vorticity in the cloud: $+0{\cdot}524$ as against $-0{\cdot}589$. Thus again we may replace the cloud by an equivalent pair of vortices and proceed as before.

To demonstrate the effect of consolidation, we show in figure 9 the horizontal momentum I_V over one wavelength (as given by equation (7.14)) calculated in the two cases when there is no consolidation of the vortices, and when there is consolidation at time $t = 6{\cdot}30$, as in figure 8. It can be seen that the difference is quite small.

Also in figure 9 we show the vortex force F_V calculated from equation (8.10). To perform the differentiation in equation (8.10) we have used the smoothed derivative $\overline{f'_n}$ given by

$$16\overline{f'_n} = [4f'_n + 3(f'_{n+1}+f'_{n-1}) + 2(f'_{n+2}+f'_{n-2}) + (f'_{n+3}+f'_{n-3})], \tag{11.7}$$

where

$$f'_n = (f_{n+1}-f_n)/\Delta t \tag{11.8}$$

for a function $f_n = f(t_n)$. Clearly this simplifies to

$$16f'_n = (f_{n+4}+f_{n+3}+f_{n+2}+f_{n+1}) - (f_n+f_{n-1}+f_{n-2}+f_{n-3}). \tag{11.9}$$

12. Energy, stability and damping

As the computation proceeds the number of point vortices below a given level, say $y = 0{\cdot}25L$, is found to increase indefinitely, and the close approach of random pairs of vortices occasions some unrealistically high values of Γ_N and dW_n/dt. As a result the computation tends to become 'noisy'. To avoid this effect we may exclude the neighbourhood of each vortex by a small circle of radius δ_n, say, inside which the velocity field is bounded.

When this is done, the total kinetic energy of the flow becomes finite. In fact by use of the formula

$$T = \frac{1}{2}\int_C \phi\, d\psi \tag{12.1}$$

for the kinetic energy within a simple closed contour C it may be shown that the total energy contained in one wavelength L is given by

$$\begin{aligned} 2T = {} & U^2L(y_\infty - k^{-1}\ln K) - 2Uk^{-1}\sum_n \Gamma_n \ln \rho_n \\ & + \sum_n \frac{\Gamma_n^2}{2\pi}\left[\ln(1/\delta_n) - \ln\frac{P}{\rho_n^{P+1}(1-\rho_n^{2P})}\right] \\ & + \sum_{m\neq n}\sum \frac{\Gamma_n\Gamma_m}{2\pi}\ln\left|\frac{W_n^P(W_n^P - \overline{W}_m^P)}{W_n^P - W_m^P}\right|. \end{aligned} \tag{12.2}$$

To make the model more plausible we assume that the radius of the core increases with the time, that is

$$\delta_n = [\epsilon(t-t_n)]^{\frac{1}{2}}, \tag{12.3}$$

where ϵ is a constant resembling the kinematic viscosity ν and $(t-t_n)$ is the elapsed time since the instant t_n when the vortex was generated. Outside the core, the velocity is assumed irrotational. Inside, following Tunstall & Inman (1974), we assume a solid rotation. Thus in the neighbourhood of $W = W_n$ the contribution of the vortex at W_n to the velocity field is assumed to be multiplied by a factor

$$1 \quad \text{when} \quad |W-W_n| > \delta_n, \tag{12.4}$$

and

$$|W-W_n|^2/\delta_n^2 \quad \text{when} \quad |W-W_n| \leqslant \delta_n. \tag{12.5}$$

The total energy of the flow, which in a completely inviscid model would tend to grow indefinitely, is to some extent kept in check by the continual increase in the size of the vortex cores. From (12.2) we see that this produces an effective rate of dissipation

$$D = \frac{d}{dt}\sum_n \frac{\Gamma_n^2}{4\pi}\ln\delta_n, \tag{12.6}$$

which by (12.3) becomes

$$D = \sum_n \frac{\Gamma_n^2}{8\pi(t-t_n)}, \tag{12.7}$$

independently of ϵ.

The last expression may be compared to the loss of energy in a system of isolated vortices in each of which

$$\psi_r \equiv \frac{\partial\psi}{\partial r} = \frac{\Gamma}{2\pi r}(1-e^{-r^2/4\nu t}), \tag{12.8}$$

where r denotes the radial distance (see Lamb 1932, p. 592). From the general formula

$$D = \iint \nu\left(\psi_{rr} - \frac{1}{r}\psi_r\right)^2 r\,dr\,d\theta, \tag{12.9}$$

we obtain

$$D = \frac{\Gamma^2}{4\pi t}\int_0^\infty \left[\frac{1-e^{-\lambda}}{\lambda} - e^{-\lambda}\right]^2 d\lambda, \tag{12.10}$$

where $\lambda = r^2/4\nu t$. The integral in (12.10) is found to equal $\frac{1}{2}$ exactly (see appendix B). This yields a value for the dissipation near the core which corresponds precisely to (12.7).

The viscous dissipation at the solid boundary $|W| = 1$ can be represented to some extent by assuming that, when $|W_n| > 1-\delta_n$, the vortex is absorbed into its image and disappears (cf. Clements 1973).

13. Coalescence of vortices

In §11 it was proposed that a cloud of point vortices sufficiently far from the boundary might be combined, at a suitable instant, into a single vortex or a vortex pair. When on the other hand each vortex is assumed to have a core of finite size, it seems natural to allow any two vortices to merge when their cores touch or overlap.

Besides providing a smoother process than before, this assumption has the advantage of keeping the total number of vortices low enough for extended computation.

Accordingly we shall assume that when two vortices at $W = W_n$ and W_m, say, (or, rather, two $2P$-fold systems of vortices) are such that

$$|W_n - W_m| < (\delta_n + \delta_m), \tag{13.1}$$

then they are replaced by a single vortex (or vortex system) of strength Γ_{nm} at the point $W = W_{nm}$ where

$$\Gamma_{nm} = \Gamma_n + \Gamma_m \tag{13.2}$$

and

$$\Gamma_{nm} \ln W_{nm}^P = \Gamma_n \ln W_n^P + \Gamma_m \ln W_m^P. \tag{13.3}$$

Moreover we assume that the *area* of the new core is the sum of the areas of the two original cores. This implies an 'age' for the equivalent core equal to $(t - t_{nm})$, where

$$\epsilon(t - t_{mn}) = \epsilon(t - t_n) + \epsilon(t - t_m). \tag{13.4}$$

Hence, we define a hypothetical time of generation for the 'equivalent' core given by

$$t_{mn} = t_m + t_n - t, \tag{13.5}$$

where t denotes the instant of coalescence.

We note that the rule (13.3) implies conservation of the total momentum. However, if Γ_n and Γ_m are nearly equal but of opposite sign, the position W_{mn} of the combined vortex may be quite far from either W_n or W_m. We therefore restrict the occurrence of coalescence to cases when $\Gamma_n \Gamma_m > 0$.

When a vortex merges with its image at the solid boundary there is little momentum change, since then $\ln W_n$ is quite small. Moreover, the loss of momentum is easily interpreted as a frictional effect (see Clements 1973).

14. Comparison with observation: the drag coefficient

It was noticed by Bagnold (1946) and confirmed by Carstens *et al.* (1969) that the fluid drag over rippled beds can greatly exceed the corresponding drag over a flat rough bottom, by some two orders of magnitude. It is interesting to compare these experimental results with our present calculations.

We may define a drag coefficient C_D by

$$\tau = C_D U |U| \tag{14.1}$$

relating the horizontal stress τ on the bottom to the instantaneous velocity U outside the (inertial) boundary layer. The mean rate of energy dissipation over a cycle will then be given by

$$\bar{D} = \overline{C_D U^2 |U|}. \tag{14.2}$$

The drag coefficient C_D may be a function of the time t, but we can define a mean drag coefficient $\bar{C}_D$ by the equation

$$\bar{D} = \bar{C}_D \overline{U^2 |U|}; \tag{14.3}$$

hence

$$\bar{C}_D = \bar{D} / \overline{|U|^3}. \tag{14.4}$$

Run no.	T (s)	$2a$ (cm)	L (cm)	$2a/L$	h/L	$\bar{C}_D$	$R_e/10^6$
			(*a*) Coarse sand (diameter 0·585 mm)				
63	3·57	20·2	14·6	1·38	·191	·120	0·20
64	3·55	24·0	16·7	1·44	·195	·133	0·27
65A	3·54	27·5	18·1	1·52	·186	·164	0·34
66	3·55	32·1	20·4	1·58	·193	·155	0·44
67	3·54	37·1	23·9	1·55	·190	·100	0·66
68	3·57	39·3	25·2	1·56	·206	·159	0·67
69	3·56	44·7	29·0	1·54	·200	·142	0·88
70	3·54	48·4	25·7	1·88	·185	·134	0·85
71	3·53	49·5	26·4	1·88	·185	·131	0·89
72	3·53	53·3	30·0	1·78	·187	·122	1·09
73	3·55	58·2	26·2	2·22	·192	·124	1·04
74	3·56	61·6	30·4	2·03	·197	·125	1·27
75	3·55	65·4	39·1	1·67	·150	·118	1·74
76	3·53	70·4	37·8	1·86	·181	·109	1·81
77	3·54	74·9	35·7	2·09	·173	·110	1·82
78	3·47	78·4	46·3	1·69	·148	·097	2·47
79	3·55	84·7	44·1	1·92	·157	·096	2·54
80A	3·54	24·9	17·4	1·43	·180	·252	2·95
			(*b*) Medium sand (diameter 0·297 mm)				
21	3·56	17·8	10·6	1·67	·171	·124	0·13
22	3·55	24·0	12·7	1·89	·175	·092	0·21
23	3·55	27·3	14·5	1·88	·176	·084	0·27
24	3·55	30·7	14·5	2·12	·179	·086	0·30
25	3·55	41·7	19·4	2·15	·170	·067	0·27
26	3·55	46·8	22·1	2·12	·162	·071	0·70
27	3·53	52·2	24·5	2·13	·132	·072	0·87
29B	3·54	64·8	27·0	2·40	·115	·053	1·19
30B	3·52	71·2	20·1	3·54	·105	·049	0·97
31B	3·52	89·0	19·1	4·66	·026	·035	1·16
32B	3·53	78·1	22·0	3·55	·065	·032	1·17
36	3·55	56·2	24·5	2·29	·131	·064	0·94
51	3·59	16·0	10·4	1·54	·183	·187	1·13
			(*c*) Fine sand (diameter 0·190 mm)				
106A	3·54	36·3	10·9	3·33	·134	·053	0·27
111A	3·53	47·4	10·6	4·49	·125	·041	0·34
112A	3·53	62·7	10·0	6·25	·048	·039	0·43
114A	3·55	22·5	10·4	1·58	·199	·092	0·12

TABLE 2. Mean drag coefficient $\bar{C}_D$ derived from the data of Carstens *et al.* (1969).

If U is sinusoidal, i.e.

$$U = U_0 \sin(\omega t + \text{constant}), \tag{14.5}$$

then we have always

$$\overline{|U|^3} = \frac{4}{3\pi} U_0^3. \tag{14.6}$$

Thus (14.4) becomes

$$\bar{C}_D = \frac{3\pi}{4} \bar{D}/U_0^3. \tag{14.7}$$

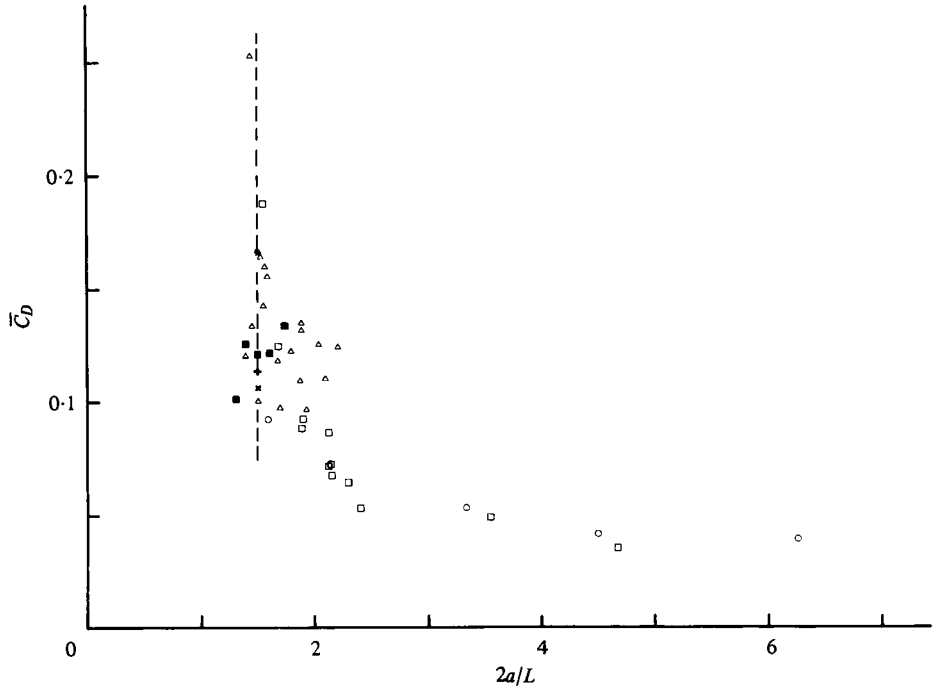

FIGURE 10. Experimental and theoretical values of the drag coefficient $\overline{C}_D$ in oscillating flow over sand ripples. Observations using various grain sizes of quartz (Carstens *et al.* 1969): △, 0·585 mm; □, 0·297 mm; ○, 0·190 mm. ■, quartz, Lofquist (1980). Present theory: ★, $\epsilon = 10^{-5\cdot5}$, ×, $\epsilon = 10^{-5\cdot0}$; +, $\epsilon = 10^{-4\cdot5}$.

(*a*) Calculated mean drag coefficients in oscillatory flow, when $P = 5$, $k = 1$, $a/L = 0{\cdot}75$

ϵ	$\overline{C}_D$	
	$0 < \omega t \leqslant 2\pi$	$\pi < \omega t < 3\pi$
0	·095	·111
$10^{-5\cdot5}$	·125	·166
$10^{-5\cdot0}$	·105	·106
$10^{-4\cdot5}$	·103	·114

(*b*) Values of the mean drag coefficient $\overline{C}_D$, when $P = 5$, $k = 1$ and $U_0 = a\omega = 1$, over various ranges of ωt

$2a/L$	ϵ	$(0, 2\pi)$	$(2\pi, 4\pi)$	$(4\pi, 8\pi)$	$(6\pi, 8\pi)$	$(8\pi, 10\pi)$	$(10\pi, 12\pi)$	Mean
1·0	10^{-5}	·091	·091	·098	·109	·084	·123	·099
1·0	10^{-4}	·093	·095	·117	·135	·137	·084	·110
1·5	10^{-5}	·101	·107	·122	·155	—	—	·121
1·5	10^{-4}	·097	·121	·169	·096	—	—	·121
2·0	10^{-5}	·091	·037	·139	—	—	—	·089
2·0	10^{-4}	·095	·098	·092	—	—	—	·095
3·0	10^{-5}	·086	·092	—	—	—	—	·089
3·0	10^{-4}	·099	·097	—	—	—	—	·098
4·0	10^{-5}	·076	—	—	—	—	—	·076
4·0	10^{-4}	·068	—	—	—	—	—	·068

TABLE 3

Bagnold (1946) measured $\bar{D}$ directly with an oscillating sand tray and defined a drag coefficient κ by

$$\kappa = \bar{\tau}/a^2\omega^2, \quad \text{where} \quad \tau = \frac{T\bar{D}}{4a}, \tag{14.8}$$

T being the period of oscillation. (We take the density of water as unity.) Since $T = 2\pi/\omega$ and $a\omega = U_0$ this definition corresponds to

$$\bar{C}_D = \tfrac{3}{2}\kappa. \tag{14.9}$$

Experimentally, Bagnold found that when $a/L < 1$ then $\kappa = 0{\cdot}08$, and, for larger values of a/L, κ decreased like $(a/L)^{-0{\cdot}75}$.

Perhaps the most complete observations of drag have been made by Carstens *et al.* with an oscillating U-tube. From their definition $\bar{\tau} = \frac{1}{8}\bar{f}U^2$ (where a single bar denotes the space-average) it is clear that we must have

$$\bar{C}_D = \tfrac{1}{8}(\bar{\bar{f}}_d - \bar{\bar{f}}_s) \tag{14.10}$$

(subscripts s and d denote the rippled bed and smooth bed, respectively). Table 2 gives those values of $\bar{C}_D$ for which the available parameters are all known. From their tables we have also deduced the values of $2a$ and $2a/L$. In figure 10 we show $\bar{C}_D$ plotted against $2a/L$. Although there is also some correlation in the data between $2a/L$ and h/L, it is fairly clear from figure 9 that the drag coefficient is relatively large at around $2a/L = 1{\cdot}5$, compared with its value at higher values of $2a/L$. The spread of values near $2a/L = 1{\cdot}5$ is also large.

The experimental points in figure 9 attributed to Lofquist (1980) tend to confirm the measurements of Carstens *et al.*

Finally in table 3 and figure 10 we show the values of $\bar{C}_D$ calculated from equations (8.14) and (14.4). Thus the second and third columns of table 2 show the values of

$$\bar{C}_D = \frac{3}{8kLU_0^2}\int_{\phi_0/\omega}^{2\pi+\phi_0/\omega} \frac{d}{dt}\left(\sum_n \Gamma_n \ln \rho_n\right) \sin \omega t \, d(\omega t) \tag{14.11}$$

calculated over the first complete cycle, centred on $\omega t = \pi$, and on the cycle centred on $\omega t = 2\pi$, respectively. The value of ϵ, as we have seen, is comparable to the kinematic viscosity ν; the boundary of the 'core' is at a radius $\delta_n = [\epsilon(t-t_n)]^{\frac{1}{2}}$, compared to the radius at which the radial velocity (12.8) is a maximum, namely $r = 2{\cdot}24(\nu t)^{\frac{1}{2}}$. We may therefore take $\epsilon = 5{\cdot}0\nu$ very roughly. In the model we took $k = 1$, $L = 2\pi/5$ and $\omega = 1$, $U_0 = 0{\cdot}75\omega L$. This gives an effective Reynolds number

$$R_e \equiv U_0 L/\nu \sim 5{\cdot}9\epsilon^{-1}. \tag{14.12}$$

The Reynolds numbers in table 3 (a) are therefore comparable with those in the experimental data of table 2.

From table 3 (a) it is evident that the calculated values of the drag coefficient $\bar{C}_D$ are not strongly dependent on ϵ. The values of $\bar{C}_D$ given in the last column have been plotted in figure 10, and are clearly within the experimental range.

At larger values of a/L, the ripple steepness, in the experiments of Carstens *et al.* (1969), on the whole decreases, so that the calculations for $P = 5$ are not directly

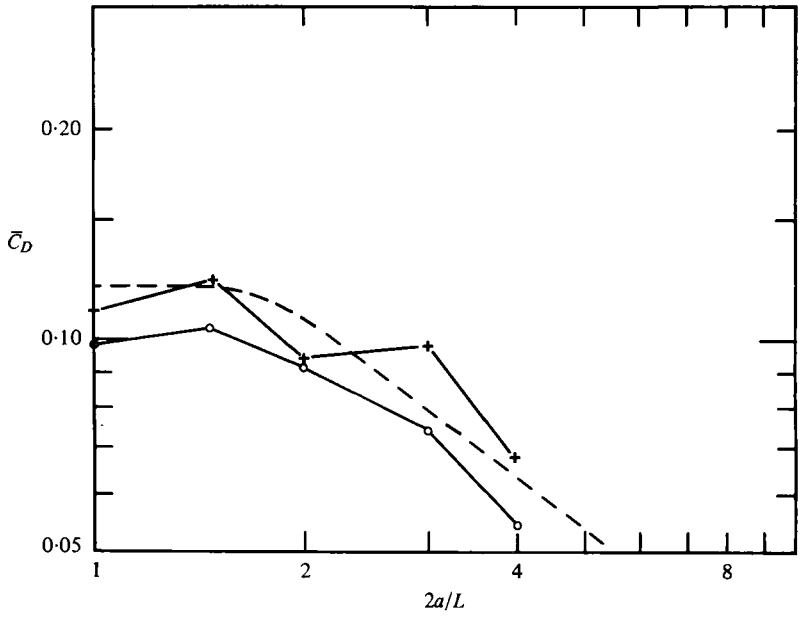

FIGURE 11. Calculated values of the drag coefficient, compared with the measurements of Bagnold (1946) over a rigid rippled bed. - - - -, observations of Bagnold (1946). Theory for $\epsilon = 10^{-4}$: +, $P = 5$; ○, $P = 6$.

comparable with their results. However, the effect of increasing a/L while maintaining h/L constant can be seen experimentally from the results of Bagnold (1946) who used a *fixed* rippled surface with a constant ripple steepness of 1/6·7, that is 0·149. His experimental curve is shown by the broken line in figure 11. This indicates that the drag tends to decrease as a/L is increased beyond 1·0. No doubt this is due to the troughs becoming filled with vorticity, so that for very long strokes an almost steady flow is achieved on each stroke.

In table 3(*b*) we show some calculated values of the mean drag coefficient $\bar{C}_D$ at various values of $2a/L$, and over successive complete cycles of the oscillation. It will be seen that even after 6 cycles the flow is not steady. Some of the scatter in the calculated values may well reflect a real unsteadiness in the flow, as has been found, for example, by Bearman, Graham & Singh (1979) with oscillating flow round cylinders. Again, the mean values of $\bar{C}_D$, shown in the right-hand column, do not appear to depend systematically on the value of ϵ. But there is a tendency for $\bar{C}_D$ to decrease as $2a/L$ increases beyond 1.

The steepness (0·149) of the ripples in Bagnold's experiment is intermediate between that for $P = 5$ and $P = 6$ (see table 1). In figure 11, the corresponding values of $\bar{C}_D$ for $P = 5$ and $P = 6$ have been plotted, at the same value of ϵ, that is $\epsilon = 10^{-4}$. It will be seen that the values for $P = 6$ all lie below those for $P = 5$, suggesting a consistent dependence on ripple steepness. Moreover each of the calculated curves shows a trend similar to Bagnold's observations.

15. Discussion and conclusions

In this study we have implicitly assumed that the ripple boundary can be regarded as stationary and well-defined, and that the effect on the flow of any sediment in suspension can be neglected, in a first approximation. In spite of these assumptions it appears that the calculated drag coefficients are in remarkably good agreement with the high values found experimentally.

It will be appreciated that fundamentally the present theory is inviscid. In the vortex-shedding analysis of §6, if the time-scale is changed by a factor τ, say, while the horizontal displacement $2a$ of the fluid for large y is kept constant, then Q is multiplied by τ^{-1} and the circulation Γ_n corresponding to a given *phase* ωt of the motion, by (6.2), is multiplied by τ^{-1} also. But Γ_n has the dimension of (length)^2/time. Hence the *displacements* associated with each vortex element are unchanged. In other words the pattern of flow is, to a first approximation independent of the frequency, for a given horizontal stroke $2a$. This agrees well with Bagnold's findings (1946, §6) that the pitch of vortex ripples was in all cases independent of the speed of oscillation.

Subsequent calculations based on assigning a 'core' to each vortex suggest that for high Reynolds numbers the drag is not strongly dependent on R_e. When computations are carried to larger values of the time t, we may expect the scatter of the computed values of $\bar{C}_D$ at any given value of ϵ to match the scatter in the observations. It is also possible that the flow may settle to an asymmetric state, the drag in one direction tending to exceed that in the opposite direction.

The limited comparisons that we have so far made with laboratory data show substantial agreement between the theoretical and observed values of the drag coefficient $\bar{C}_D$. They are also in rough agreement with the field data quoted by Vitale (1979, table 1; Vitale's friction coefficient f, defined as $3\pi\bar{D}/2U_0^3$, is equivalent to $2\bar{C}_D$).

A more detailed comparison with the available observations, for different values of P, $2a/L$ and ϵ will be given in future papers, together with a theory of the *stability* of sand ripples making use of the present model, or a simplified version of it, for the fluid flow. The question of possible three-dimensional vortex flows associated with Bagnold's 'brick-pattern' (1946, figure 8) remains also to be investigated.

Meanwhile it should be mentioned that the basic transformation of the ripple surface into a polygon, as described in §2, is by no means confined to integral values of P, but can be used whenever P is rational, i.e.

$$P = N/M \geqslant 2, \tag{15.1}$$

where N and M are any positive integers. Thus in (2.2) we should have

$$kNL = 2M\pi, \tag{15.2}$$

that is, the P-gon encloses its centre M times, and in both the ζ plane and the W plane we map N ripple lengths onto M sheets of a Riemann surface. The case $P = 11/2$ is illustrated in figure 12. The analytic expressions, which need not be set out in detail, are all quite similar to those already given.

The special case $P = 2$ corresponds to a *digon* or, in the z plane, a set of equally spaced vertical parallel plates. The corresponding conformal transformation of a flat

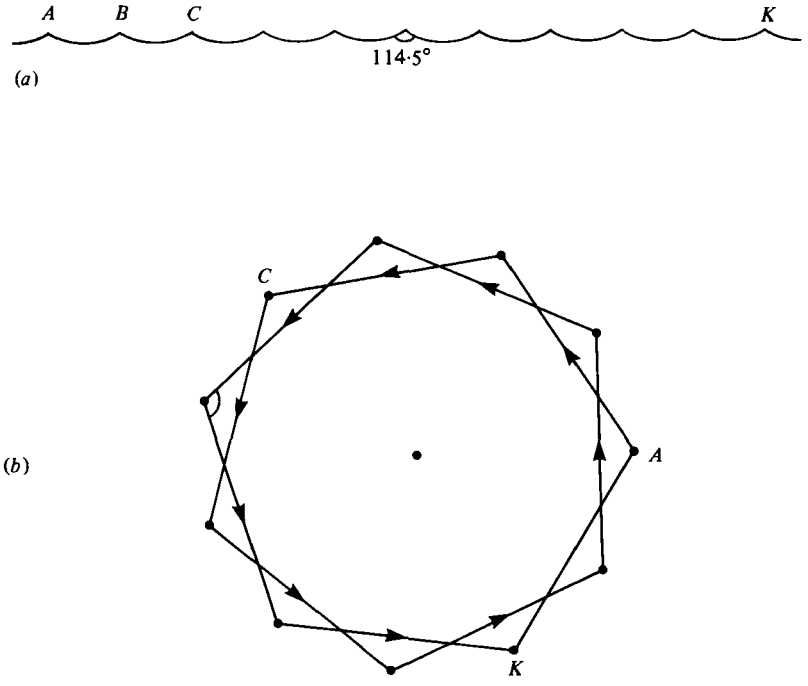

FIGURE 12. The transformation of 11 ripples with crest angle 114·50° into the polygon $\{11/2\}$, (*a*) in the z plane and (*b*) in the ζ plane.

(two-dimensional) plate into a circular cylinder, i.e.

$$\zeta = \zeta_0 - \int_{W_0}^{W} \frac{1-W^2}{W^2}\,dW, \tag{15.3}$$

is well known. For then $K = \frac{1}{2}$ (see table 2) and on taking $\zeta_0 = W_0 = 1$ we obtain

$$\zeta = \tfrac{1}{2}(W + W^{-1}). \tag{15.4}$$

The author is indebted to his colleagues Dr I. G. Jonsson, Dr I. A. Svendsen and Dr B. Hansen for arousing his interest in sand ripples during a visit to Copenhagen in January 1979. Valuable assistance in amassing the literature on this topic was given by the Librarian at the Institute for Hydraulic Research (I.S.V.A.) at Lyngby.

A further stimulus for this work came from papers presented at the Coastal Engineering Conference in Sydney in March 1980. I have had useful discussions on vortex shedding with Dr P. Saffmann (Pasadena), Dr H. G. Hornung (Canberra), Dr J. Fenton (Sydney) and Dr T. Sarpkaya (Monterey); and on sand ripples with Dr P. Nielsen (Sydney), Dr K. E. B. Lofquist (Washington, D.C.), Dr J. W. Kamphuis (Kingston) and Dr J. F. A. Sleath and Mr C. G. deK. du Toit (Cambridge). It is a pleasure to acknowledge their help and interest.

A preliminary account of these results was presented at the 7th International Conference on Numerical Methods in Fluid Dynamics, held at Stanford, California, from June 23 to 27, 1980.

Appendix A. Derivation of (8.5) from Blasius' theorem

We start from Blasius' theorem in the form

$$F+iG=\tfrac{1}{2}i\left[\int_{C_1}\left(\frac{d\chi}{dz}\right)^2 dz\right]^*+i\int_{C_1}\frac{\partial\chi}{\partial t}dz+\frac{\partial\psi}{\partial t}\int_{C_1}dz. \tag{A 1}$$

Here $F+iG$ is the force exerted by the fluid on the boundary C_1 of the ripple. The signs in (A 1) are the reverse of those normally assumed, since in figure 6 the contour C_1 is taken with the solid to the right, not to the left.

Consider first

$$J_1\equiv\int_{C_1}\left(\frac{d\chi}{dz}\right)^2 dz, \tag{A 2}$$

where χ is given by equation (5.4). Since $d\chi/dz$ is periodic in x, it follows that the integral of $(d\chi/dz)^2$ taken along the two vertical contours C_2 and C_4 in figure 6 just vanishes. So by Cauchy's theorem

$$J_1=-\int_{C_3}\left(\frac{d\chi}{dz}\right)^2 dz+\sum_n\int_{B_n}\left(\frac{d\chi}{dz}\right)^2 dz, \tag{A 3}$$

where B_n denotes a small contour surrounding z_n. But, on C_3, $d\chi/dz\sim U$, and on B_n we may write

$$\frac{d\chi}{dz}\sim\frac{\Gamma_n}{2\pi i}\frac{1}{z-z_n}+\dot{z}_n, \tag{A 4}$$

where $\dot{z}_n$ is the velocity of the vortex at z_n. Hence

$$J_1=LU^2+\sum_n\int_{B_n}\left(\frac{\Gamma_n}{2\pi i}\frac{1}{z-z_n}+\dot{z}_n\right)^2 dz=LU^2+2\sum_n\Gamma_n\dot{z}_n, \tag{A 5}$$

by the residue theorem.

Likewise let

$$J_2\equiv\int_{C_1}\frac{\partial\chi}{\partial t}dz. \tag{A 6}$$

Then if the Γ_n are all independent of t we have

$$J_2=\int_{C_1}\left[\frac{\dot{U}}{ik}\ln W-P\sum_n\frac{\Gamma_n}{2\pi i}\left(\frac{W_n^{P-1}\dot{W}_n}{W^P-W_n^P}-\frac{\overline{W}_n^{P-1}\dot{\overline{W}}_n}{W^P-\overline{W}_n^P}\right)\right]dz. \tag{A 7}$$

Now on C_2 and C_4 we have

$$\ln W=\ln\rho\pm i\pi/P, \tag{A 8}$$

and on C_3

$$\ln W\sim\ln K-\ln\zeta=\ln K+ikz. \tag{A 9}$$

Hence

$$\begin{aligned}\int_{C_1}\ln W dz&=-\int_{-h}^{y_\infty}(2i\pi/P)\,i\,dy+\int_{-\frac{1}{2}L+iy_\infty}^{\frac{1}{2}L+iy_\infty}(\ln K+ikz)\,dz\\&=(2\pi/P)(y_\infty+h)+L(\ln K-ky_\infty)\\&=L(ky+\ln K).\end{aligned} \tag{A 10}$$

Moreover on C_3

$$\frac{W_n^{P-1}\dot{W}_n}{W^P-W_n^P}-\frac{W_n^{P-1}\dot{\overline{W}}_n}{W^P-\overline{W}_n^P}\sim-\frac{\dot{W}_n}{W_n}+\frac{\dot{\overline{W}}_n}{\overline{W}_n}=-2\frac{\dot{\rho}_n}{\rho_n}, \tag{A 11}$$

and the residue of the integrand at $z = z_n$ is simply

$$-\frac{\Gamma_n}{2\pi i}\frac{W_n}{W_n'} = -\frac{\Gamma_n}{2\pi i}\dot{z}_n. \tag{A 12}$$

Hence we have

$$J_2 = -iL\dot{U}(h + k^{-1}\ln K) + \frac{PL}{\pi i}\sum_n \Gamma_n \frac{\dot{\rho}_n}{\rho_n} - \sum_n \Gamma_n \dot{z}_n. \tag{A 13}$$

Thirdly we have

$$J_3 \equiv \frac{\partial \psi}{\partial t}\int_{C_1} dz = L\frac{\partial \psi_s}{\partial t} \tag{A 14}$$

where ψ_s is found from (7.10):

$$\frac{\partial \psi_s}{\partial t} = -P\sum_n \frac{\Gamma_n}{2\pi}\frac{\dot{\rho}_n}{\rho_n}. \tag{A 15}$$

Hence

$$J_3 = -k^{-1}\sum_n \Gamma_n \dot{\rho}_n/\rho_n. \tag{A 16}$$

Altogether then we find from (A 1)

$$\begin{aligned} F + iG &= \tfrac{1}{2}iJ_1^* + iJ_2 + J_3 \\ &= (\tfrac{1}{2}iLU^2 + i\sum_n \Gamma_n \dot{z}_n) + L\dot{U}(h + k^{-1}\ln K) \\ &\quad + \left(2k^{-1}\sum_n \Gamma_n \frac{\dot{\rho}_n}{\rho_n} - i\sum_n \Gamma_n \dot{z}_n\right) - k^{-1}\sum_n \Gamma_n \frac{\dot{\rho}_n}{\rho_n} \\ &= \tfrac{1}{2}iLU^2 + L\dot{U}(h + k^{-1}\ln K) + k^{-1}\sum_n \Gamma_n \frac{\dot{\rho}_n}{\rho_n}. \end{aligned} \tag{A 17}$$

The real part of this equation gives precisely (8.5).

Appendix B. Evaluation of (12.10)

To show that

$$M \equiv \int_0^\infty \left(\frac{1 - e^{-\lambda}}{\lambda} - e^{-\lambda}\right)^2 d\lambda = \tfrac{1}{2}, \tag{B 1}$$

we have

$$M = M_1 - 2M_2 + M_3, \tag{B 2}$$

say, where

$$M_1 = \int_0^\infty e^{-2\lambda}\, d\lambda = \tfrac{1}{2}, \tag{B 3}$$

$$\begin{aligned} M_2 &= \int_0^\infty \frac{(1 - e^{-\lambda})e^{-\lambda}}{\lambda}\, d\lambda \\ &= \lim_{L\to\infty}\int_0^L \left(\frac{1 - e^{-2\lambda}}{\lambda} - \frac{1 - e^{-\lambda}}{\lambda}\right) d\lambda \\ &= \lim\left[\int_0^{2L}\frac{1 - e^{-\mu}}{\mu}\, d\mu - \int_0^L \frac{1 - e^{-\lambda}}{\lambda}\, d\lambda\right] \\ &= \lim\int_L^{2L}\frac{1 - e^{-\mu}}{\mu}\, d\mu = \ln 2 \end{aligned} \tag{B 4}$$

and

$$M_3 = \int_0^\infty \frac{1-2e^{-\lambda}+e^{-2\lambda}}{\lambda^2}\,d\lambda$$
$$= \int_0^\infty \frac{2(1-\lambda-e^{-\lambda})-(1-2\lambda-e^{-2\lambda})}{\lambda^2}\,d\lambda$$
$$= \lim_{L\to\infty}\left[\int_0^L \frac{2(1-\lambda-e^{-\lambda})}{\lambda^2}\,d\lambda - 2\int_0^{2L}\frac{(1-\mu-e^{-\mu})}{\mu^2}\,d\mu\right],$$

where $\mu = 2\lambda$. Thus

$$M_3 = -2\lim_{L\to\infty}\int_L^{2L}\frac{(1-\lambda-e^{-\lambda})}{\lambda^2}\,d\lambda$$
$$= 2\lim\int_L^{2L}\frac{1}{\lambda}\,d\lambda = 2\ln 2. \tag{B.5}$$

From equations (B 2)–(B 5) the result (B 1) follows immediately.

REFERENCES

Abramowitz, M. & Stegun, I. A. 1965 *Handbook of Mathematical Functions*. Dover.

Aref, H. 1979 Motion of three vortices. *Phys. Fluids* **22**, 393–400.

Ayrton, H. 1910 The origin and growth of ripple-mark. *Proc. Roy. Soc.* A **84**, 285–310.

Bagnold, R. A. 1946 Motion of waves in shallow water. Interaction between waves and sand bottoms. *Proc. Roy. Soc.* A **187**, 1–15.

Bearman, P. W., Graham, J. M. R. & Singh, S. 1979 Forces on cylinders in harmonically oscillating flow. In *Mechanisms of Wave Induced Forces on Cylinders* (ed. J. H. Shaw). Pitman.

Bijker, E. W., van Hijum, E. & Vellinga, P. 1976 Sand transport by waves. *Proc. 15th Conf. on Coastal Engng, Hawaii*, pp. 1149–1167.

Carstens, M. R., Nielson, F. M. & Altinbilek, H. D. 1969 Bed forms generated in the laboratory under oscillatory flow. *Coastal Engng Res. Center, Fort Belvoir, Va., Tech. Mem.* no. 28.

Clements, R. R. 1973 An inviscid model of two-dimensional vortex shedding. *J. Fluid Mech.* **57**, 321–336.

Clements, R. R. & Maull, D. J. 1975 The representation of sheets of vorticity by discrete vortices. *Progr. Aerospace Sci.* **16**, 129–146.

Graham, J. M. R. 1980 The forces on sharp-edged cylinders in oscillatory flow at low Keulegan–Carpenter numbers. *J. Fluid Mech.* **97**, 331–346.

Inman, D. L. 1957 Wave-generated ripples in nearshore sands. *Beach Erosion Board, Washington, Tech. Mem.* no. 100.

Kajiura, K. 1968 A model of the bottom boundary layer in water waves. *Bull. Earthquake Res. Inst., Univ. of Tokyo* **46**, 75–123.

Kalkanis, G. 1964 Transport of bed material due to wave action. *Coastal Engng Res. Center, Fort Belvoir, Va., Tech. Mem.* no. 2.

Kiya, M. & Arie, M. 1977 A contribution to an inviscid vortex shedding model for an inclined flat plate in uniform flow. *J. Fluid Mech.* **82**, 223–240.

Lamb, H. 1932 *Hydrodynamics*, 6th edn. Cambridge University Press.

Lofquist, K. E. B. 1978 Sand ripple growth in an oscillatory-flow water tunnel. *Coastal Engng Res. Center, Fort Belvoir, Va., Tech. Paper* no. 78–5.

Lofquist, K. E. B. 1980 Observations of drag on naturally rippled sand beds under oscillatory flows. *Proc. 17th Conf. on Coastal Engng, Sydney, Australia* (in press).

Longuet-Higgins, M. S. 1973 On the form of the highest progressive and standing waves in deep water. *Proc. Roy. Soc.* A **331**, 445–465.

MOGRIDGE, G. R. & KAMPHUIS, J. W. 1972 Experiments on bed form generation by wave action. *Proc. 13th Conf. on Coastal Engng, Vancouver, B.C.*, pp. 1123–1142.

NEHARI, L. 1952 *Conformal Mapping*. McGraw-Hill.

NIELSEN, P. 1979 Some basic concepts of wave sediment transport. *Inst. of Hydraulics and Hydraulic Engng, Tech. Univ. of Denmark, Lyngby, Series Paper* no. 20.

PRANDTL, L. & TIETJENS, O. G. 1934 *Fundamentals of Hydro and Aeromechanics* (translated by L. Rosenhead). Dover.

RAMSEY, A. S. 1942 *Hydromechanics*. Part II. *Hydrodynamics*. Cambridge University Press.

SAFFMAN, P. G. & BAKER, G. R. 1979 Vortex interactions. *Ann. Rev. Fluid Mech.* **11**, 95–122.

SLEATH, J. F. A. 1975 A contribution to the study of vortex ripples. *J. Hydraulic Res.* **13**, 315–328.

STANSBY, P. K. 1977 An inviscid model of vortex shedding from a circular cylinder in steady and oscillatory far flows. *Proc. Inst. Civil Eng.* **63**, 865–880.

TUNSTALL, E. B. & INMAN, D. L. 1974 Vortex generation of oscillatory flows over rippled surfaces. *J. Geophys. Res.* **80**, 3475–3484.

VITALE, P. 1979 Sand bed friction factors for oscillatory flows. *Proc. A.S.C.E.* **105** (WW3), 229–245.